Journal of Controlled Release 383 (2025) 113743

Contents lists available at ScienceDirect

Journal of Controlled Release

journal homepage: www.elsevier.com/locate/jconrel

Local controlled release of stabilized monoclonal antibodies☆

Rae Sung Chang [a,1], Jennifer Walker [a,1], Anzar A. Mujeeb [b], Padma Kadiyala [b], Karthik Pisupati [a], Jeffrey Jamison [c], Anna Schwendeman [a], Yusuf Haggag [a,d], David A. Antonetti [e], Maria G. Castro [b], Steven P. Schwendeman [a,f,*]

[a] Department of Pharmaceutical Sciences and the Biointerfaces Institute, University of Michigan, Ann Arbor, MI 48109, USA
[b] Department of Neurosurgery and Department of Cell and Developmental Biology, University of Michigan School of Medicine, Ann Arbor, MI 48109, USA
[c] Ophthy-DS, Inc., Kalamazoo, MI 49009, USA
[d] Department of Pharmaceutical Technology, Faculty of Pharmacy, Tanta University, Tanta, Egypt
[e] Department of Ophthalmology and Visual Sciences, University of Michigan, Ann Arbor, MI 48105, USA
[f] Department of Biomedical Engineering, University of Michigan, Ann Arbor, MI 48109, USA

ARTICLE INFO

Keywords:
PLGA implant
Monoclonal antibody
Stability
Local controlled release
Wet AMD
Glioblastoma

ABSTRACT

Monoclonal antibody (mAb) therapeutics have become widely successful for treatment of any number of diseases. However, for certain hard-to-reach tissues, e.g., eye, brain, tumors, and joints, local delivery is desired and long-term controlled release is necessary to avoid frequent injections and poor patient compliance. If local and sustained exposure of mAbs (or their Fab or nanobody fragments) could be accomplished by injectable polymer long-acting release (LAR) systems, the incredible potential of mAb therapeutics could be extended to additional diseases, e.g., neovascular age-related macular degeneration (wet AMD) and glioblastoma multiforme (GBM). In prior studies, long-acting delivery of mAbs has been limited by the inability to design a delivery system prepared from a biodegradable polymer used in FDA-approved LARs that achieves long-term continuous release of structurally stable and immunoreactive mAb with a low initial burst release that is easily injectable and avoids material build-up upon repeated injection. Here, we present for the first time a long-acting delivery system capable of delivering several different mAbs for multiple indications by developing a novel process to stabilize mAbs through the combination of formulation, micronization and encapsulation conditions, and to control stabilized mAb exposure in vivo for months by formulation with an appropriate biodegradable polymer (poly (lactic-*co*-glycolic acid) (PLGA)), utilization of a pH- and pore-modifying agent, and development of a novel PLGA coating layer to control osmotic pressure induced by elevated levels of critical co-encapsulated stabilizers, particularly mAb-stabilizing-trehalose. The resulting implants showed long-term efficacy in animal models for both wet AMD and GBM after single local injections. Although much more work needs to be done before their clinical application to these two diseases, the injectable PLGA platform meets several important benchmarks for controlled mAb delivery and can be developed further for delivery of a wide array of mAbs and other cofactors, offering an improved therapeutic option for treating diseases amenable to local antibody therapy.

One Sentence Summary: A generalizable injectable biodegradable PLGA implant platform for site-specific and long-term slow and continuous release of stabilized monoclonal antibody drugs demonstrates improved in vivo efficacy for wet AMD and glioblastoma.

1. Introduction

Monoclonal antibody (mAb) therapeutics have become a powerful drug class recently occupying five out of ten spots on the current US drug sales list [1]. Unlike many biologics, mAbs typically have longer circulating plasma half-lives owing to the neonatal Fc receptor-mediated recycling mechanism [2]. MAbs encompass diverse pharmacologic targets and have been successfully administered systemically. Certain

☆ This article is part of a Special issue entitled: 'SI Feijen' published in Journal of Controlled Release.

* Corresponding author at: Department of Pharmaceutical Sciences and the Biointerfaces Institute, University of Michigan, Ann Arbor, MI 48109, USA.
E-mail address: schwende@umich.edu (S.P. Schwendeman).

[1] These authors contributed equally to this work

https://doi.org/10.1016/j.jconrel.2025.113743
Received 31 October 2024; Received in revised form 9 April 2025; Accepted 15 April 2025
Available online 17 April 2025

tissues such as the eye, brain, solid tumors, and joints are difficult to attain therapeutic mAb levels without inducing significant off-target side effects [3,4]. The eye and the brain, for example, possess protective endothelial barriers and surrounding blood vessels comprising the blood-retinal and blood-brain barriers, respectively. These barriers preclude optimal and effective treatment for a multitude of diseases such as neovascular age-related macular degeneration (also referred to as wet AMD) and glioblastoma (GBM).

Wet AMD is one of the most common causes of blindness [5–8] and may be treated with monthly intravitreal injections of an anti-vascular endothelial growth factor (VEGF) mAb such as Avastin® (bevacizumab, Genentech), Lucentis® (ranibizumab, Genentech) or the VEGF trap, Eylea® (aflibercept, Regeneron) [5,9,10]. More recently, Vabysmo™ (Faricimab, Genentech) is the first bispecific antibody that inhibits both angiopoietin-2 (Ang-2) and (VEGF-A) for the treatment of wet AMD or diabetic macular edema (DME) [11]. Despite the inherently long intravitreal half-life of bevacizumab, the monthly injections are problematic, posing risks of infection, inflammation and hemorrhage [12]. Additionally, monthly injections are a real burden on patients leading to compliance issues [13]. An injection frequency of at least 3-months between doses is a highly desired clinical goal [14–16].

Glioblastoma (GBM) is one of the most deadly cancers with a high rate of recurrence and a poor median survival (14–20 months), which has not greatly improved over the past several decades [17–19]. Due to the immunosuppressive nature of GBM, immune checkpoint inhibitor immunotherapies such as anti-PD-1 and anti-CTLA-4 blockade are currently being investigated as a treatment option. However, systemic administration of these antibodies is associated with adverse side effects [18,20–23]. Local controlled release of immune checkpoint inhibitors for GBM offers the potential of superior local drug exposure while avoiding systemic toxicity and mitigating systemic immunosuppression [22].

An approach to overcome such biological barriers to drug delivery is the application of biodegradable polymer implants capable of releasing the drug from weeks to months after local delivery. Intravitreal injections in the physician's office [24] or implantation after tumor resection [25] are common applications of this strategy. Other examples that focus on local/regional controlled-release of drugs in general include intravaginal rings releasing contraceptives and preventive drugs for sexually transmitted diseases [26,27], drug-eluting stents for the treatment of peripheral artery disease [28,29], and intra-articular extended release formulations for osteoarthritis knee pain [30]. Collectively, these diseases demonstrate an unmet need and significant opportunity to develop generalizable approaches for sustained, local release of mAbs. However, mAbs as proteins are often unstable when encapsulated and slowly released from polymers [31]. General strategies for slow and continuous release of mAbs from poly(lactic-*co*-glycolic acid) (PLGA), the most common polymer used in FDA-approved long-acting release (LAR) products, have not been achieved. Most mAb LAR formulations previously reported are deficient in one or more of these important categories: high and efficient loading of mAb [32–35], low initial burst release (<20 %) [34,36], >80 % total mAb release [31–33,35–39], >1-2 month of release [32,34–36,40–42], extensive analyses of mAb structural stability and activity during formulation and during release [32–35,37,38,40–43], a lack of polymer build-up after drug release [44], and evaluation of mAb tolerability and efficacy in vivo [32–34,36–46].

To address this challenge we selected bevacizumab contained in Avastin® [47,48] as a model mAb, and developed a LAR formulation approach based on injectable pencil-lead sized, sub millimeter-scale rods like the Ozurdex® implant [49]. We built this formulation based on multiple protein-stabilizing features such as incorporating pH modifying and pore-forming agents (e.g., $MgCO_3$ and $Mg(OH)_2$), elevated protein loading, and use of anhydrous encapsulation previously developed for other PLGA-encapsulated albumin and growth factors [50,51]. We found that stabilization of bevacizumab required high levels of osmotic excipients, such as trehalose, to halt aggregation during micronization of the mAb for anhydrous encapsulation, although inclusion of the excipient caused rapid mAb release. By applying a novel, micron-thin, PLGA coating we averted the full immediate mAb release from the high mAb/excipient loaded PLGA core implant and achieved long-term continuous mAb release with minimal loss of protein stability. After optimizing our bevacizumab LAR implant specifically for bevacizumab stability and release kinetics, we then demonstrated the generality of this strategy for delivery of four additional mAbs, human and murine forms of anti-PD-1 and anti-CTLA-4. Here we present our unique mAb encapsulation technique, implant composition, in vitro performance and demonstration of this approach in vivo efficacy for wet AMD and GBM indications.

2. Methods

2.1. Materials

The Avastin® commercial solution of bevacizumab was purchased from the University of Michigan pharmacy and used within its shelf-life period. PLGA 50:50 (inherent viscosity = 0.64 dL/g and M_w = 54.3 kDa, ester terminated) was purchased from LACTEL Absorbable Polymers (Birmingham, AL). Trehalose dihydrate (trehalose), $MgCO_3$ (basic), guanidine hydrochloride, DL-dithiothreitol (DTT), ethylenediaminetetraacetic acid (EDTA), Na_2HPO_4, NaH_2PO_4, anti-human IgG-alkaline phosphatase antibody produced in goat and *p*-nitrophenyl phosphate liquid substrate system (pNPP) were purchased from Sigma-Aldrich Chemicals (St. Louis, MO). Tween 80 (10 %), acetone, KH_2PO_4, K_2HPO_4, KCl, phosphate buffered saline (PBS), Amicon Ultra-15 Centrifugal Filter Units (10,000 MWCO), and coomassie plus reagent assay kit were purchased from Fisher Scientific (Hanover Park, IL). Platinum-cured silicone rubber tubing (0.8 mm i.d., 2.4 mm o.d.) was purchased from Cole Parmer (Vernon Hills, IL). Recombinant human vascular endothelial growth factor (VEGF) was a generous gift from Genentech. Murine and human anti-PD-1 and anti-CTLA-4 mAbs were a generous gift from Bristol-Myers Squibb.

2.2. Preparation of mAb powder

The buffer of Avastin® solution containing bevacizumab and excipients was exchanged into 51 mM sodium phosphate buffer (pH 6.2) by using Amicon Centrifugal Filter Units (10,000 MWCO) to remove trehalose. Then, different levels of trehalose were added (weight of trehalose:weight of bevacizumab = 0, 0.1, 0.5, 1 and 1.5:1) and the solution was diluted with 51 mM sodium phosphate buffer (pH 6.2) for the final bevacizumab concentration of 25 mg/mL and lyophilized. The solid was then ground by CryoMill (Retsch, Germany) at 30 Hz for 30 min and sieved through 90-μm screen (Newark Wire Wearing, Newark, NJ). Anti-PD-1 and anti-CTLA-4 powders were prepared in the same way with a ratio of trehalose:mAb of 1.5:1 *w*/w. High trehalose content protein powder was prepared (ratio of 2.4:1 w/w, trehalose:bevacizumab) by lyophilization of the commercial Avastin® solution without buffer exchanging, followed by grinding and sieving (<90 μm).

2.3. Preparation of mAb injectable implants

The resulting mAb powder was suspended into 50 % (*w*/w) PLGA solution in acetone with 3 % (w/w) $MgCO_3$ in a 2 mL centrifuge tube, then mixed and transferred into a 3 mL syringe. The suspension was extruded into silicone rubber tubing (i.d. = 0.8 mm) and sealed at the ends with paperclips, then dried at room temperature for 48 h followed by vacuum drying at 40 °C and 23 in. Hg vacuum for an additional 48 h. The final dried implants were obtained by removal of silicone tubing and were cut into 0.5 cm long segments for future use. For coated implants, the core implants were put back into silicone tubing and pure PLGA solution at various concentrations (10 %, 30 %, 50 %) in acetone within

a 3 mL syringe was extruded over the core implants to coat the surface, and the tubing was sealed at both ends before drying in vacuum oven at room temperature for 48 h and at 40 °C for an additional 48 h. Then, silicone tubing was removed, and the final coated implants were cut to 0.5 cm for the following experiments. For anti-PD-1 and anti-CTLA-4 implants, coating was repeated after drying for a total of two, 30 % PLGA in acetone coatings, before silicone tubing removal.

2.4. Preparation of sterile mAb injectable implants

For an initial test of biocompatibility, the optimal coated implants with bevacizumab were prepared aseptically using sterile starting materials. Tubes, syringes, filters, silicone rubber tubing and containers were either received sterile or autoclaved. The aqueous solutions were sterile filtered. The $MgCO_3$ and polymer were dry heat sterilized (150°C, 23 in Hg, 3 h) in nylon sterile bags. Components were combined in a sterile hood and placed in pre-sterilized nylon sterilization bags, freeze-drying (protein solutions) and vacuum drying (base and coated cylinders).

2.5. Measurement of mAb loading in implants

Implants (3–5 mg) were dissolved in 1 mL of acetone for 1 h and centrifuged to precipitate mAb. PLGA dissolved in supernatant was removed and the mAb pellet was washed with acetone and centrifuged three times more to remove residual PLGA. The pellet was then air dried, reconstituted in 1 mL of PBST (phosphate buffered saline with 0.02 % Tween-80, pH 7.4) at 37 °C overnight and analyzed by size-exclusion high-performance liquid chromatography (SE-HPLC) or size-exclusion ultra-performance liquid chromatography (SE-UPLC). The condition of SE-HPLC to quantify monomer and soluble aggregates was followed as previously described [52] with slight modifications, which included the injection volume of 50 μL and filtration of all samples through 0.45 μm filter. Similarly, loading was determined for anti-PD-1 and anti-CTLA-4 after polymer removal by SE-UPLC with an injection volume of 10 μL, a flow rate of 0.4 mL/min through a BEH SEC 450 Å, 2.5 μm column (Waters, Milford, MA) over 6 min, and elution was monitored at UV absorption of 280 nm. For both SE-HPLC and SE-UPLC, an isocratic elution of mobile phase (0.182 M KH_2PO_4, 0.018 M K_2HPO_4, and 0.25 M KCl, pH 6.2). Extracted loading and loading efficiency were calculated by the following Eqs. (1) and (2):

$$\text{Extracted loading (\%)} = \frac{\text{Weight of extracted bevacizumab}}{\text{Weight of total implant}} \times 100\% \quad (1)$$

$$\text{Loading efficiency (\%)} = \frac{\text{Extracted loading}}{\text{Theoretical loading}} \times 100\% \quad (2)$$

2.6. In vitro release of mAb from implants

Implants (0.5 cm long, unless otherwise indicated) were added in 1.5 mL centrifuge tubes with 1 mL of PBST and incubated at 37 °C without agitation, as agitation was found to cause insoluble aggregation of the antibody in the release media. The release medium was replaced with fresh medium at each time point. The amount of released mAb at each time point was measured by SE-HPLC/UPLC as described above and calculated as percentage of the released amount out of the extracted loading of soluble mAb. In certain instances, the release media was also analyzed for protein structure and immunoreactivity, as described below.

2.7. Evaluation of residual bevacizumab in implants

At the end of release study, the remaining bevacizumab was extracted by the same procedure used to measure protein loading after lyophilizing the remaining polymer. The protein pellet was then reconstituted in PBST and incubated at 37 °C overnight to determine the soluble fraction of the protein remained in the polymer. After centrifugation, the supernatant was collected and the remaining insoluble precipitates were dissolved in denaturing solvent (6 M guanidine hydrochloride/1 mM EDTA) at 37 °C for 1 h to determine non-covalent protein aggregates [51]. After centrifuging and collecting supernatant, the remaining insoluble precipitates were dissolved again in denaturing/reducing solvent (6 M guanidine hydrochloride /1 mM EDTA/10 mM DL-dithiothreitol) to measure covalent protein aggregates formed by disulfide bonds. Concentration of protein aggregates in each step was measured by Coomassie plus protein assay. All measurements were performed in triplicate ($n = 3$) and bevacizumab standards were dissolved in the same solvent used for each analysis.

2.8. Measurement of the effect of trehalose on aggregation of bevacizumab in dry powder for encapsulation

Bevacizumab powder with the various weight ratios of trehalose to bevacizumab (0, 0.1, 0.5, 1, 1.5 and 2.4:1) were dissolved in PBST at 37 °C overnight. The soluble fraction of protein was measured by SE-HPLC to determine the effect of trehalose on aggregation of bevacizumab.

2.9. Confocal microscopy

The distribution of protein powder and PLGA coating in the coated implants was visualized using confocal microscopy. A commercial Alexa Fluor® 488-labeled BSA (Thermo Fisher Scientific, Waltham, MA) was used instead of bevacizumab to ensure high intensity of fluorescence. Regular BSA including 5 % of the fluorescent BSA was loaded at 10 % with trehalose and $MgCO_3$ into core implants as described before. To visualize and distinguish the PLGA coating from the fluorescent protein, Cyanine5 carboxylic acid dyes (Cy5, Lumiprobe, Hallandale Beach, FL) were dissolved at 10 μg/mL in PLGA/acetone solution, and the core implants were coated with the Cy5/PLGA solution as previously described. The dried implants were cut for cross-sectional images and placed on a clean glass slide. A clean glass cover slide was placed over the implant slices. To visualize lateral surface of implants, the dried or lyophilized implants from in vitro release study were placed on a glass slide. Samples were imaged using a confocal microscope (Nikon A1 Spectral Confocal Microscope) with excitation/emission wavelengths of 488/525 nm for the BSA labeled with Alexa Fluor® 488 and 640/700 nm for the Cy5 in PLGA coating.

2.10. Measurement of monomer content

Intact bevacizumab originally shows a small dimer peak in SE-HPLC chromatogram and the monomer content calculated by the following Eq. (3),

$$\text{Monomer content (\%)} = \frac{\text{AUC of a monomer peak}}{\text{AUC of total peaks}} \times 100\% \quad (3)$$

is dependent on the concentration of bevacizumab. Similarly, monomer content was calculated based on SE-UPLC for anti-PD-1 and anti-CTLA-4.

2.11. Enzyme linked immunosorbent assay (ELISA) and cell-based bioassay

The ELISA was performed to determine immunoreactivity of the released bevacizumab as described previously [41] with some modifications. Briefly, 96-well ELISA microplates were pre-coated with 50 μL of VEGF (0.5 μg/mL) solution in PBS (phosphate buffered saline, pH 7.4) at 4 °C overnight. After washing with 350 μL of PBS four times, 100 μL of PBS containing 1 % BSA (bovine serum albumin) was added for blocking

and incubated at room temperature for 2 h. After washing, 50 μL of bevacizumab standards (0–2.56 μg/mL) and samples diluted in PBST containing 1 % BSA were added into each well and incubated at room temperature for 1 h. After washing, 50 μL of secondary antibody (alkaline phosphatase conjugated goat anti-human IgG) was added at 1: 1000 dilution in PBST containing 1 % BSA into each well and incubated for another 1 h. Detection was carried out by adding 50 μL of pNPP after washing. Color development was monitored with a plate reader (Dynex MRX II, Richfield, MN) every 10 min for 30 min at 405 nm.

Immunoreactivity and bioactivity for anti-PD-1 and anti-CTLA-4 were determined using commercial ELISA kits from AcroBiosystems (Newark, DE, EPH-V1 and ECH-V1, respectively) or with a cell-based assay from Promega (Madison, WI, J1250 and JA3001, respectively) with slight modifications. Briefly, the competitive ELISAs used human PD-1 and human CTLA-4 as the coating ligands, then an equal parts mixture of release samples ($n = 3$ for each time point, triplicated on the plate, diluted to ~1 μg/mL) and biotin labeled anti-PD-1 or anti-CTLA-4 were added to the coated plates and were detected by UV absorption at 450 nm after HRP conjugation using TMB substrate.

For the anti-PD-1 cell-based bioassay, human PD-L1 expressing aAPC/CHO-K1 cells were cultured overnight (37 °C, 5 % CO_2) on a 96-well plate. The next day, standards and release samples were added to the cells followed by the addition of PD-1 effector cells (Jurkate T cells expressing human PD-1 and a luciferase reporter, NFAT response element) and incubate for 6 h (37 °C, 5 % CO_2). For the anti-CTLA-4 bioassay, CTLA-4 effector cells (Jurkate T cells expressing human CTLA-4 and a luciferase reporter), standards and release samples, and aAPC/Raji cells expressing CD80 and CD86 ligands were plated on a 96-well plate and incubated for 6 h (37 °C, 5 % CO_2). Standards were prepared using the same solutions of mAbs, provided by Bristol-Myers Squibb, that were used to make the mAb implants. Release samples were run in triplicate and concentration of reactive mAb was calculated based on the standard curve. Both bioassays were detected using the Bio-Glo Luciferase assay system (Promega, Madison, WI) using a 0.5 s integration time, and standards were graphed using a 4-parameter logistic curve for interpolating the release sample concentrations. For each release time point, $n = 3$, each replicate was triplicated on the plate.

Immunoreactivity of all three mAbs (and bioactivity of anti-PD1 mAb) were calculated by the following eq. (4):

$$\text{Immunoreactivity} \Big/ \text{bioactivity (\%)} = \frac{\text{Concentration from ELISA/bioactivity}}{\text{Concentration from SE} - \text{HPLC/UPLC}} \times 100\% \quad (4)$$

2.12. Circular dichroism spectroscopy (CD)

CD was performed with Jasco J-815 CD spectrometer equipped with Jasco temperature controller (CDF-426S/15) and Peltier cell at 25 °C. The samples were diluted or buffer-exchanged into 51 mM sodium phosphate buffer (pH 6.2) and concentrated by using Amicon Centrifugal Filter Units (10,000 MWCO), so the final concentration ranged from 0.05 to 0.5 mg/mL for far UV measurements (200–250 nm). The samples were measured in quartz cuvettes (Hellma) with a path length of 1 mm. The spectra were collected in continuous mode at a speed of 50 nm/min, bandwidth of 1 nm and a DIT of 1 s and were the averages of 5–10 scans. The spectrum of blank 51 mM sodium phosphate buffer (pH 6.2) was subtracted from each spectrum by using the Jasco spectra manager software (Version 2.1). The raw data was converted to mean residue ellipticity (MRE, $\theta_{mrw,\lambda}$) using the following eq. (5):

$$[\theta]_{mrw,\lambda} = MRW \times \frac{\theta_\lambda}{10 \times d \times c} \quad (5)$$

where is the θ_λ observed ellipticity in degree at wavelength λ, d is the path length in cm, c is the concentration in g/mL, and mean residue weight (MRW), calculated as the molecular weight of the mAb divided by the number of amino acids −1, in g/mol is 113 for bevacizumab, 112 for anti-CTLA-4, and 110 for anti-PD-1. Concentration of the total protein measured by SE-HPLC/SE-UPLC was used to normalize all data. Data smoothing was performed using SigmaPlot software (Version 12.0, Systat Software, Inc.).

2.13. Evaluation of anti-VEGF efficacy in a DL-AAA-induced rabbit chronic retinal leakage model

Anti-VEGF efficacy of the sterile PLGA-bevacizumab implants was examined in the rabbit DL-AAA (alpha-aminoadipic acid) induced chronic retinal vascular leakage model [53,54]. Dutch Belted Rabbits were purchased from Covance (1.0–1.2 kg). Animals were sedated with isoflurane vapors to effect. The cornea was anesthetized with 1–2 drop of proparacaine and rinsed with ophthalmic betadine prior to intravitreal injection. On day 0, all animals received 80 μL of an 80 mM DL-AAA solution per eye intravitreally. Starting on week 10, animals were imaged to ascertain baseline leakage. Tropicamide and Eyeprine were used to dilate the eye and animals were sedated with isoflurane vapors to effect. IR fundus imaging, fluorescein angiography (FA), were performed using the Heidelberg Spectralis cSLO. Eyes were anesthetized with proparacaine and pupils dilated with tropicamide. 50 μL to 25 % sodium fluorescein was injected into the marginal ear vein and allowed to circulate for >5 min. FA images of the entire vasculature were collected, exported and placed into Power Point (Microsoft), arranged into a single coherent collage and graded for leakage. Once the retina developed stable leakage (>10 weeks), the mAb implants (average 400 μg of mAb/implant) were injected into the rabbit vitreous using a 16G thin-wall needle and a Hamilton syringe plunger. To compare with free mAb, the same dose of Avastin® solution (400 μg, 16 μL) was injected into the free mAb control group. The control group received only saline (16 μL). At each time point (day 3, 7, 14 and every other week), FA was performed and leakage from the retinal blood vessels on the FA images was scored at 14 points across the fundus by a trained expert. Peripheral vessels were graded on a score of 0–4 and central vessels were graded on a score of 0–1. This resulted in a potential maximum score of 50 per eye. The scoring criteria are described in Supplementary Table 1. The raw scores from each time point were normalized to the initial score of each eye. The statistical analysis was done with Stata 15, a mixed-effects regression model with fixed effects for day and group, and their interaction. To account for the dependence within animals and within eyes, a random intercept for each eye was nested within a random intercept for each animal. To test for significant differences at each time point, marginal means were compared between each group.

2.14. Evaluation of anti-VEGF efficacy in a VEGF-induced rabbit retinal leakage model

Anti-VEGF efficacy of the PLGA-bevacizumab implants was examined in the rabbit VEGF-induced retinal vascular leakage model (male Dutch Belted rabbits, 2 animals, 4 eyes, 8 blood vessels/group). The 30 % PLGA coated implants (400 μg of bevacizumab) were injected into the rabbit vitreous. To compare with free mAb, the same dose of Avastin® solution was injected as a control group. The no-treatment control group received no drug. On day 42, recombinant human VEGF (1000 ng) was intravitreally injected (29-30G needle) into each eye to induce retinal leakage. On day 45, fluorescein angiography (FA) was performed and the degrees of fluorescein leakage and tortuosity of retinal blood vessels were scored on 4-point scale as described in Supplementary Table 2. On days 56 and 70, the same assay was performed for the implant group. For these time points, two untreated rabbits were added as a new control group at each time point and the previous no-treatment control and free mAb groups were not tested further since their retinal blood vessels were

damaged during the 42-day VEGF challenge.

2.15. Biocompatibility of bevacizumab intravitreal implants

An initial testing of biocompatibility of sterile bevacizumab-loaded PLGA implants (30 % PLGA coated implants (400 μg of bevacizumab)) was investigated using healthy rabbits (male Dutch Belted rabbits, 6 animals, 12 eyes). Implants were injected intravitreally as described above. The rabbits were euthanized after 70 days and the collected eyes were immediately stored in 10 % neutral buffered formalin. The posterior chambers were injected with 0.3 mL of formalin at the limbus upon receipt by the ULAM In-Vivo Animal Core at the University of Michigan. Eyes were trimmed on midline in the dorso-ventral plane and each half hemisphere was separately placed in a histology cassette, labeled A and B. All cassettes were processed to paraffin using standard histologic protocols. Step sections were cut at midline (3 sections) and at 2 mm off-midline (3 sections) and mounted on glass slides. Each section was 4 μm thick. One slide at each level was stained with hematoxylin and eosin on an automated histostainer by routine protocols. Histological sections were evaluated using light microscopy at magnifications ranging from x20 to x600 by a board-certified veterinary pathologist using an Olympus BX45 light microscope (Olympus Corporation). Slides were evaluated with knowledge of the right or left eye for each animal but blinded to treatment status. All regions of the eye (optic nerve, retina [all layers], choroid, iris/ciliary body/iridal angle, vitreous/posterior chamber, lens, aqueous/anterior chamber, cornea, and other areas (sclera, conjunctival or other visible periocular structures) were examined. Severity scoring parameters were defined in the supplementary Table 3.

2.16. Determining therapeutic efficacy in a syngeneic GBM model

Intracranial GBM tumors were established in 6–8-week old C57BL/6 mice by stereotactically injecting 3.0×10^4 GL261 cells into the right striatum using the following coordinates: 1.00 mm anterior, 2.5 mm lateral, and 3.00 mm deep from the bregma [55].

At 7 days post-tumor implantation, mice were divided into two experimental sets. The first set received the following treatments: saline, systemic IP administration of anti-CTLA4, IR (radiotherapy), a combination of anti-CTLA4 with IR, and anti-CTLA4 sterile implants combined with IR. The second set received saline, blank implants, blank implants with IR, systemic administration of anti-PD1 + IR, and anti-PD1 implants with IR. The IR dose used for this study was 2 Gy, 5 days/week for 2 weeks, totaling 20 Gy of ionizing radiation. For local delivery, each implant was loaded with 285 μg of anti-PD1 or anti-CTLA4 neutralization antibody, designed to release approximately 5 μg of antibody per day over a span of 57 days. For systemic delivery, anti-CTLA4 and anti-PD1 antibodies were administered intraperitoneally (IP) at a dosage of 5 μg/day for up to 60 days or until the survival endpoint was reached. These dosing regimens were chosen to ensure consistent and therapeutically relevant delivery of the antibodies in both local and systemic treatment groups. MAb-containing and blank PLGA rods were intratumorally implanted. Mice were monitored for tumor burden and survival, and upon observing symptoms of tumor burden mice were perfused with paraformaldehyde (PFA).

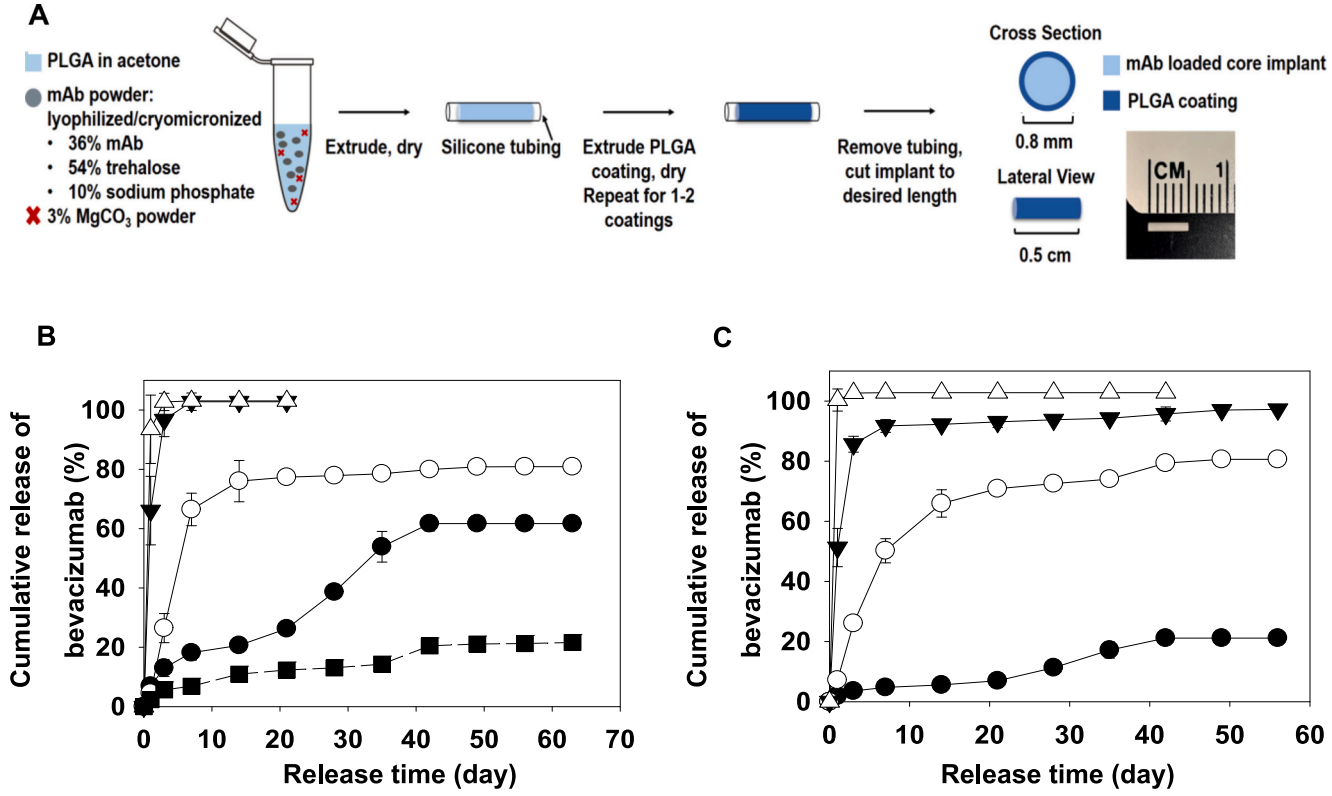

Fig. 1. Implant preparation and release kinetics of bevacizumab under physiological conditions in vitro. (A) Implant preparation schematic with representative views of the implant and actual image of implant after PLGA coating. Uncoated implants were prepared with (B) original Avastin® powder (solid line) and buffer-exchanged bevacizumab powder without trehalose (dashed line), and with (C) buffer-exchanged bevacizumab powder with the ratio of 1.5:1 *w*/w trehalose: bevacizumab. Theoretical loading of bevacizumab in each formulation was 3 % (●), 6 % (○), 10 % (▼), 15 % (△, ■). Actual extracted loading of implants is listed in Supplementary Tables 2 and 4. Symbols represent mean ± SE, $n = 3$. Error bars not present when smaller than symbols.

3. Results

3.1. Optimization of stabilizing excipient content in PLGA-bevacizumab LAR

Injectable PLGA 50/50 rods were formed by suspending lyophilized and cryo-micronized mAb powder (<90 μm) with solid micron-sized $MgCO_3$ in an acetone/PLGA solution before extrusion into 0.8 mm i.d. silicone tubing and removal of organic solvent [51,52] (Fig. 1A). As Avastin® contains a significant level of osmotically active and release-modifying excipients [56] (Supplementary Table 4), particularly trehalose, we adjusted both the composition and level of mAb powder in the formulation. As seen in Fig. 1B, the release kinetics under physiological conditions from these preparations suffered from rapid release over the first few days (i.e., high initial burst) when the mAb content was desirably >6 % *w*/w, and below this level, the protein was slowly released without complete release owing to insoluble protein aggregation [51]. Complete removal of trehalose from the powder resulted in low encapsulation efficiency (Supplementary Table 5), very slow and incomplete release, e.g., 12.9 % total cumulative mAb release with 41.9 % insoluble aggregation even at 15 % theoretical mAb loading (Supplementary Table 6 and Fig. 1B).

To identify the conditions for adequate protein stability during encapsulation we initially monitored the level of mAb aggregation as a function of the content of the stabilizer, trehalose, by size-exclusion chromatography (SEC) after cryo-micronization. As seen in Supplementary Fig. 1, a critical level of trehalose (1.5:1, trehalose:mAb, *w*/w), which was slightly below the level in the commercial formulation (2.4:1), was necessary to halt significant protein aggregation. Reducing trehalose below this level induced significant aggregation of mAbs (Supplementary Fig. 2), which is undesirable for release and likely more immunogenic [57]. Reducing the osmotic excipient to 1.5:1, trehalose:mAb, in the powder at elevated mAb content (10 %) resulted in implants, prepared as above, with reduced osmotic pressure and initial burst. However, the long-term release was still not continuous, and protein aggregation was still evident as the total protein release was <<100 % of loaded protein after several weeks (Fig. 1C).

3.2. PLGA coating over core implant, in vitro release and stability characterization

Trehalose is known to stabilize proteins in the solid state by multiple mechanisms including, vitrification, water-replacement, and preferential exclusion [58,59]. Therefore, the mAb powder with just enough trehalose (1.5:1, trehalose:mAb, *w*/w) was encapsulated as before Fig. 1A, except with a PLGA coating (from 10, 30 and 50 % w/w PLGA in acetone, Supplementary Tables 7 and 8) around the core implant to further manage the osmotic burst release triggered by the necessary trehalose stabilizer (Supplementary Fig. 3). As seen in Fig. 2D and E, the coating was only microns thick (Supplementary Table 8). Applying a thicker coating layer (achieved by using a higher polymer concentration in coating solution) over a 10 % mAb loaded core implant, the burst release began to disappear and extensive mAb release (>89 % for 30 % polymer in acetone coating solution) was achieved for >6 weeks (Fig. 2A, Supplementary Table 9). Increasing the PLGA coating to a 50 % polymer solution resulted in a slightly lower total cumulative release (82 %). This reduced total release in the thicker coated sample is consistent with the slightly higher levels of mAb aggregation and protein recovery (Supplementary Table 9), likely owing to lower microenvironmental pH created by slower release of acid byproducts from the core matrix by thicker coating, which inhibits release of acidic degradation products. Increasing mAb core implant loading to 15 %, with a 50 % PLGA solution coating, still resulted in high initial burst release and complete release in the first few days (Supplementary Fig. 3). To determine if mAb released from the optimized coated implants (10 % mAb core implant loading, and 30 or 50 % coating) retained stability,

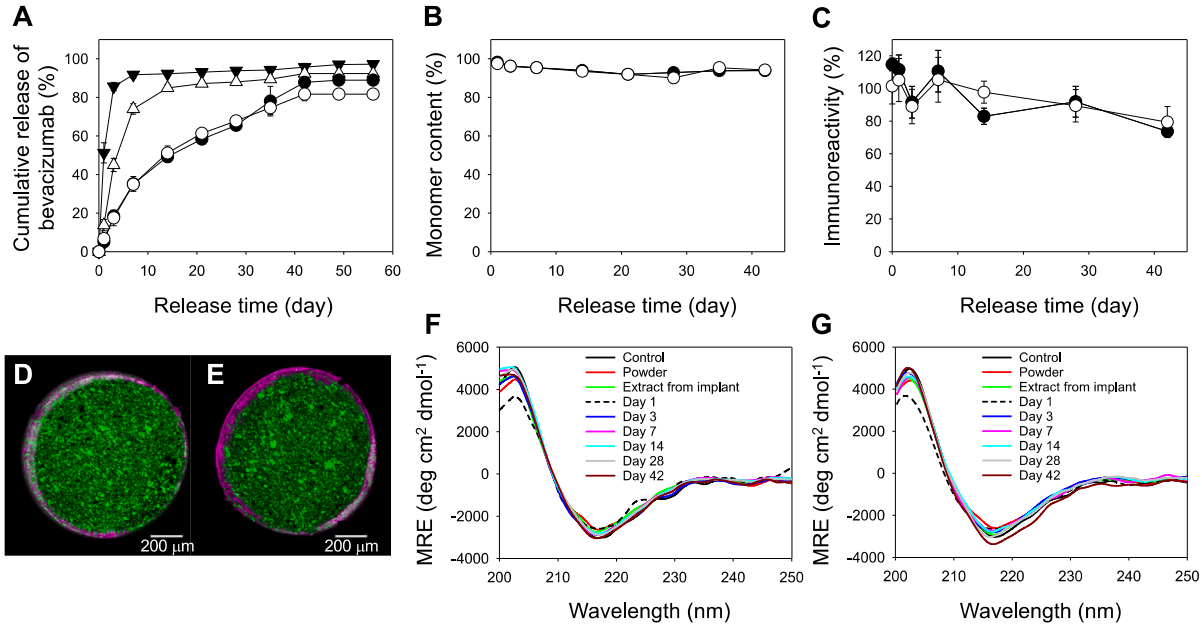

Fig. 2. In vitro characterization of the coated implants. (A) Release kinetics of bevacizumab from uncoated (▼) and coated (△, ●, ○) implants prepared with 10 % initial theoretical loading of bevacizumab in buffer-exchanged mAb powder with 1.5:1 *w*/w trehalose:bevacizumab in the core implants. Concentrations of PLGA solution for coating were 10 % (△), 30 % (●), and 50 % (○). Symbols represent mean ± SE, $n = 3$. (B) monomer content and (C) immunoreactivity of released bevacizumab from implants (10 % mAb loading in core implant) coated with 30 % w/w PLGA (●) and 50 % PLGA (○). Symbols represent mean ± SE, n = 3. Cross-sectional confocal microscopic images of (D) 30 % and (E) 50 % PLGA coated implants (green: Alexa Fluor® 488-labeled BSA powder, purple:PLGA coating). CD spectra of mAb from intact Avastin® solution(Control), 1.5:1 powder formulation, extracts and release samples of (F) 30 % PLGA and (G) 50 % PLGA coated implants (10 % mAb loading in core implant). Error bars not shown when smaller than symbols. (For interpretation of the references to color in this figure legend, the reader is referred to the web version of this article.)

the protein was also analyzed by size exclusion chromatography (SEC), circular dichroism (CD) spectroscopy, and VEGF-binding enzyme-linked immunosorbent assay (ELISA). As seen in Fig. 2B, C, F, and G, the mAb was remarkably stable according to these assays in the polymer, retaining >90 % monomer, secondary structure (indicated by insignificant changes in characteristic β-sheet peak), and > 80 % immunoreactivity over 6 weeks.

3.3. Bevacizumab implant in vivo performance

Anti-VEGF efficacy of the optimized mAb implant (10 % mAb core loading, 30 % PLGA coating, 0.5 cm length) was compared to the same dose (400 μg) of free mAb in a rabbit DL-alpha-aminoadipic acid (DL-AAA) induced chronic retinal leakage model [53,54]. After a single intravitreal injection, the mAb implant strongly protected retinal blood vessels over 12 weeks, as seen by inhibition of retinal leakage, determined by scoring of fluorescein angiography images with normalization to their initial scores. The free mAb group showed significant anti-VEGF efficacy for only 4 weeks before returning to the no-treatment control leakage level (Fig. 3).

Similar long-term exposure of the anti-VEGF mAb was observed after control, free mAb, and mAb implant intravitreal injection into healthy rabbit eyes before intravitreal challenge with exogenous VEGF (1000 ng). Six weeks after intravitreal injection of the bevacizumab formulations, only the mAb implant groups protected retinal blood vessels against VEGF challenge, while significant leakage was observed in the no-treatment control and free mAb groups. The retinal blood vessels of the implant group were still protected over 8 weeks, but not at 10 weeks when leakage finally appeared (Fig. 4). The difference between protection times observed for the two rabbit models likely relates to the aggressive VEGF challenge in the healthy animals, which may require higher intravitreal mAb levels to inhibit leakage than do DL-AAA rabbits. The vitreous, which is known to bind bevacizumab [60], is known to extend the anti-VEGF exposure significantly with an intravitreal half-life of 4.9 days (human) [61] and 4.3 days (rabbit) [60], far beyond that predicted during in vitro release.

3.4. Biocompatibility of the injectable coated bevacizumab/PLGA implant in vivo

To examine for potential adverse events, the histology of eyes after 70 days after a single intravitreal implant injection were examined in healthy rabbits. Results of in vivo biocompatibility of the coated bevacizumab/PLGA implants showed 3 out of 6 rabbits in this group had no histological findings in either eye. The other three animals had mild (n = 2) and moderate (n = 1) findings in one eye, but the affected eye varied from animal to animal (Supplementary Tables 10A and 10B). Principal findings, where present, showed mild to moderate retinal detachment/degeneration, mild to moderate focal intravitreal inflammatory cell (macrophage) infiltrates, and focal intravitreal debris consistent with the presence of the degrading implant (Supplementary Fig. 4). These findings suggested a mild macrophagic "clean-up" response to the degrading implant. Collectively, these histological findings suggested excellent biocompatibility of the coated mAb/PLGA implants after a single intravitreal injection.

3.5. Immune checkpoint inhibitor implant in vitro release and stability characterization

Although ocular delivery of anti-VEGF drugs is significant, an even

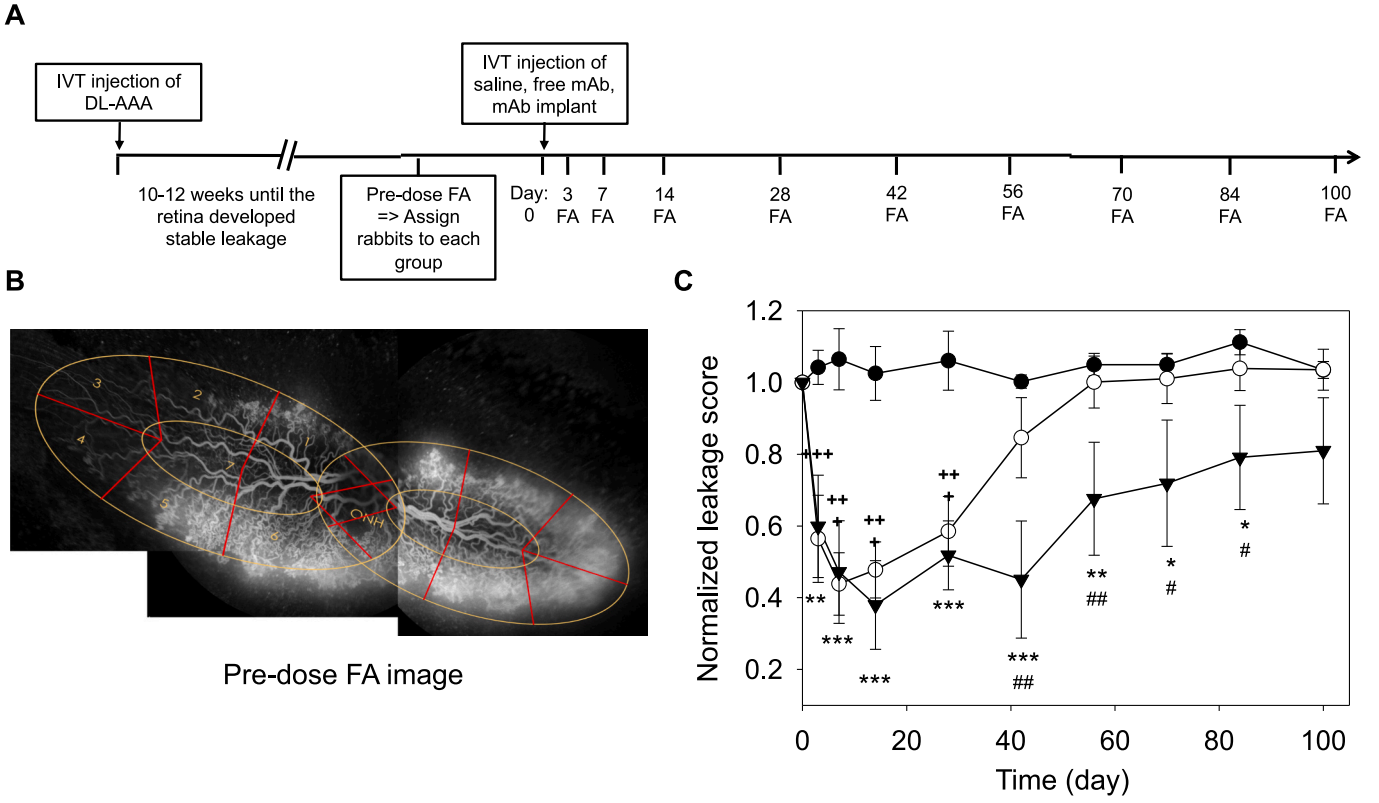

Fig. 3. Anti-VEGF efficacy of bevacizumab implants in a rabbit DL-AAA induced chronic retinal leakage model. (A) Schematic representation of the rabbit study timeline. (B) Representative fluorescein angiography (FA) image of pre-dose retinal blood vessel for leakage scoring. (C) Normalized leakage scores for 100 days. Symbols (●: saline, ○: free bevacizumab, ▼: bevacizumab implant) represent mean ± SE. (+++: $p < 0.001$, ++: $p < 0.01$ for saline-free bevacizumab, *: $p < 0.05$, **: $p < 0.01$, ***: $p < 0.001$ for saline-bevacizumab implant, #: $p < 0.05$, ##: $p < 0.01$, ###: $p < 0.001$ for free bevacizumab-bevacizumab implant). Statistical analysis was performed with Stata 15 software.

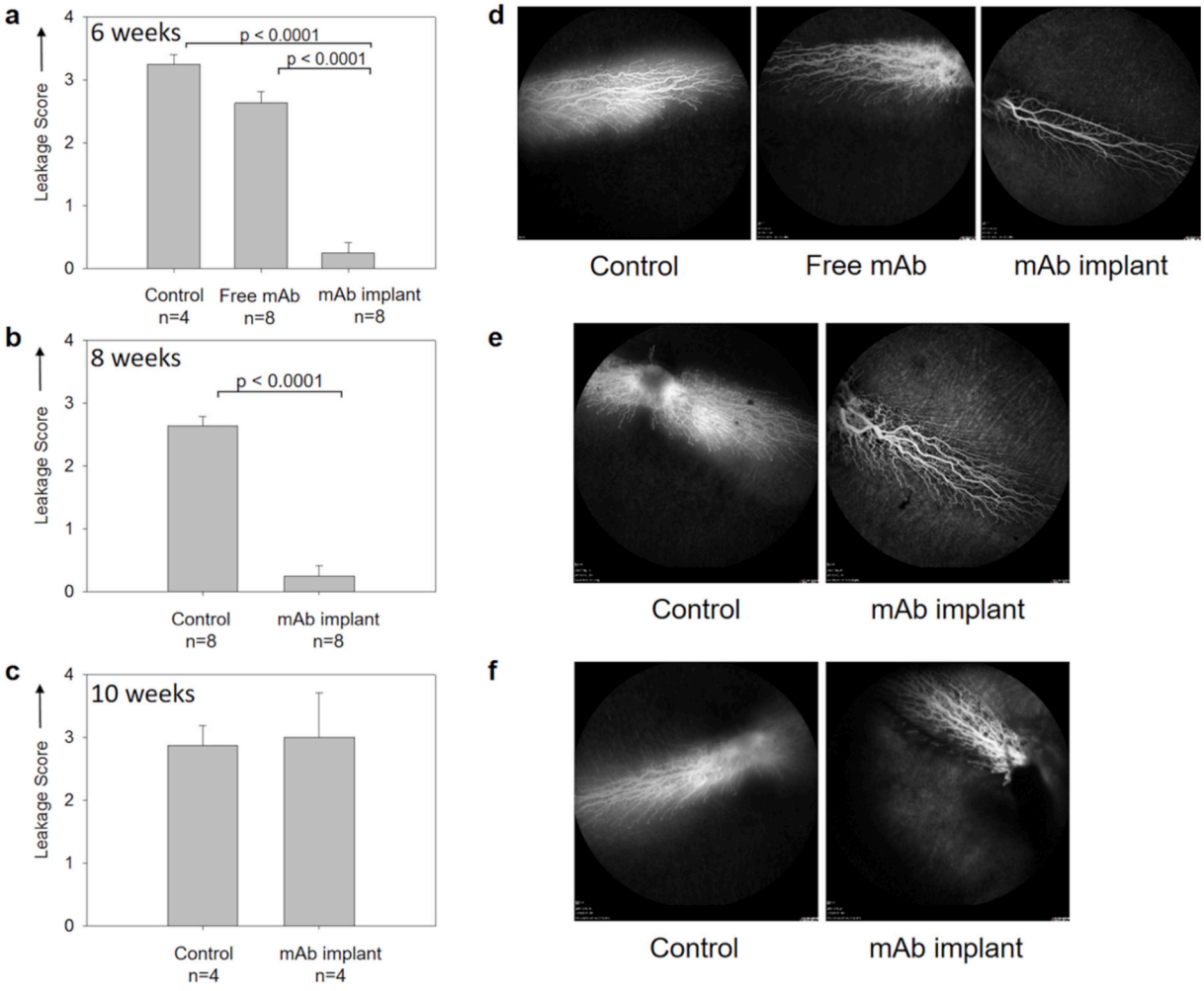

Fig. 4. Anti-VEGF efficacy of mAb implant in the rabbit VEGF-induced retinal leakage model 6, 8 and 10 weeks after intravitreal injection of mAb implant or free mAb compared to untreated control (no drug). a) leakage scores and d) representative FA images of untreated control, free mAb treated, and mAb implant treated rabbits 6 weeks after treatments. b) leakage scores and e) representative FA images of untreated control, and mAb implant treated rabbits 8 weeks after treatments. c) leakage scores and f) representative FA images of untreated control, and mAb implant treated rabbits 10 weeks after treatments. Bars represent mean ± SE for replicates indicated in each graph.

higher impact could be envisaged if the mAb-releasing PLGA formulation could be applied to important therapeutic mAbs for additional difficult-to-reach tissues and diseases such as brain cancer. To test this potential and the generality of our formulation approach, we encapsulated two key immune checkpoint inhibitor mAbs, anti-PD-1 and anti-CTLA-4, using the same formulation (albeit with a second PLGA coating to improve uniformity, Fig. 1A), and investigated their controlled release and stability properties. The two human mAbs are FDA-approved and administered systemically to treat a variety of cancers including melanoma, non-small-cell lung cancer, renal-cell carcinoma, and squamous-cell carcinoma of the head and neck [62–64]. In addition to challenges in reaching the brain, systemic administration of immune checkpoint mAbs suffers from unwanted side effects mainly in the gastrointestinal tract, endocrine glands, skin, and liver [64].

As seen in Fig. 5, both murine and human forms of anti-PD-1 and anti-CTLA-4 could be encapsulated (6–8 % loading, Supplementary Table 11) and released continuously for ~60 days, similar to that observed with bevacizumab. As with the anti-VEGF mAb, the immune checkpoint mAbs were released in a monomeric form in each case until the very end of the release period when small levels of soluble aggregates (<0.66–5.18 % of total) were observed in anti-PD-1 implants (Fig. 5B). The structure and immunoreactivity of released mAbs were also well-preserved, insofar as determined by far UV CD and ELISA (Figs. 5C-E). Some loss of immunoreactivity was noted during release for both mAbs, which is reasonable considering the excipients applied from the bevacizumab formulation were not optimized for these immune checkpoint antibodies. The immunoreactivity results were in-line with cell-based bioactivity evaluations for days 1 and 28 (Supplementary Fig. 5).

3.6. *In vivo therapeutic efficacy of systemic vs. local controlled delivery of immune checkpoint blockade inhibitors*

To determine whether the long-acting mAb polymers could have application to treat brain cancer, we inserted murine immune checkpoint mAb implants via intratumoral injection through a 1.5 mm diameter burr hole in a syngeneic GBM bearing mouse. Since radiation therapy (IR) is the standard-of-care for GBM patients [18,23], we combined a single insertion of the controlled release mAb implant therapy with IR. The murine forms of the mAbs were used in place of the human forms to offset interspecies immunogenicity to the mAbs.

Immunocompetent C57BL/6 mice were implanted with glioma cells in the right striatum. Following the surgical implantation of tumors, the mice were observed daily for 10 days to monitor their recovery Subsequently, the mice were monitored regularly for clinical signs of tumor burden, such as weight loss, hunched posture, scruffy fur, neurological

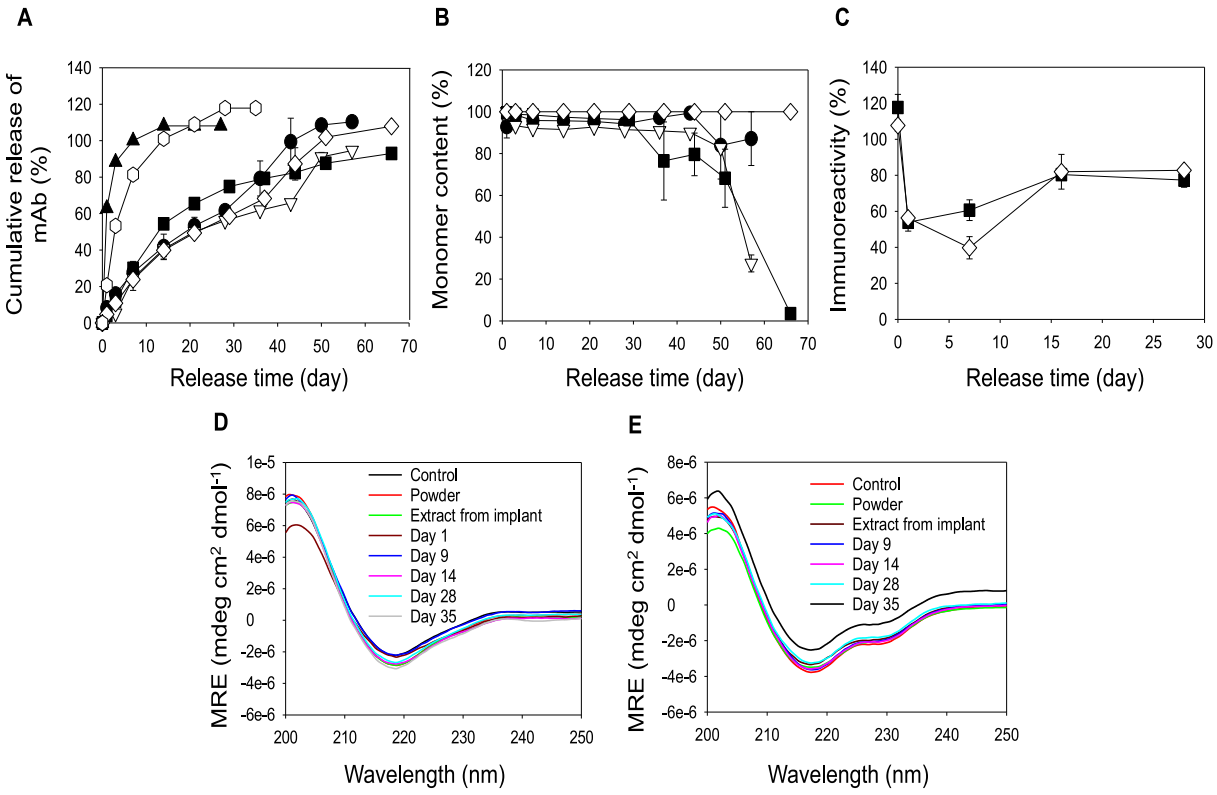

Fig. 5. In vitro characterization of the twice coated implants. (A) Release kinetics and (B) monomer content of twice coated mAb implants from murine anti-PD-1 (●), murine anti-CTLA-4 (▽), human anti-PD-1 (■), and human anti-CTLA-4 (◇), and release kinetics for once coated implants of human anti-PD-1 (▲) and human anti-CTLA-4 (⬡). Symbols represent mean ± SE, $n = 2$ for murine and mean ± SE, $n = 3$ for human mAb samples. (C) Immunoreactivity by ELISA of human anti-PD-1 (■) and human anti-CTLA-4 (◇). Symbols represent mean ± SE, $n = 4$–6. (D,E) CD spectra of (D) human anti-CTLA-4 and (E) human anti-PD-1 from extract and release media compared to 1.5:1 (trehalose:mAb, *w*/w) powder formulation and control antibody (anti-PD-1 day 1 release concentration was too low for analysis). Error bars not shown when smaller than symbols.

symptoms, or reduced activity. The reported treatments were administered concurrently with two cycles of radiotherapy, the established standard treatment for GBM (Figs. 6A and 7A).

As seen in Fig. 6, intraperitoneal (IP) administration of soluble anti-CTLA4 antibodies (Median survival, MS = 34-day post-implantation) at an equivalent dosing rate to the local implants did not affect median survival compared to the saline-treated group (MS = 32); IR alone (MS = 33) also did not affect the survival. In addition, the group treated with IP anti-CTLA4 combined with radiation (MS: 43 days post-implantation) was found to be nonsignificant ($p < 0.1$) (Fig. 6B). The group treated with anti-CTLA4 implants combined with radiation (MS: 76 days post-implantation) showed an approximate 2.7-fold increase ($p < 0.05$) in median survival (MS) compared to the saline group (Fig. 6B).The median survival of blank implants (MS = 34 days post-implantation) and blank implants in combination with radiation (MS = 35 days post-implantation) also displayed a undesirably similar median survival (Fig. 7B). Among mice treated with IP soluble anti-PD-1+ IR (MS: 35 days) and those treated with anti-PD-1 coated implants combined with IR (MS: 71 days post-implantation) ($p < 0.1$) (Fig. 7B), there was a 2-fold increase in the median survival. These findings collectively indicate significant in-vivo efficacy of combining implants loaded with immune checkpoint blockade inhibitors with radiotherapy to enhance survival in a preclinical model of GBM.

4. Discussion

4.1. Addressing an unmet need for local biodegradable polymer controlled release of mAbs

There is an increasing demand for new and improved monoclonal antibody (mAb) therapeutics and approaches for their delivery to the body owing to the rising prevalence of a number of diseases (e.g., macular degeneration, cancer, and osteoarthritis), rising healthcare expenditures and longer life expectancy. Unlike other biologics, mAbs encompass an incredible diversity of pharmacologic targets and have been successfully administered systemically because of their unusually long plasma half-lives [2]. However, certain tissues such as the eye, brain, solid tumors, and joints are difficult to attain therapeutic mAb levels without inducing significant off-target side effects [3,4]. The eye and the brain, for example, possess protective endothelial barriers and surrounding blood vessels comprising the blood-retinal and blood-brain barriers, respectively. These barriers preclude optimal and effective treatment for a multitude of diseases such as neovascular age-related macular degeneration (also referred to as wet AMD) and glioblastoma (GBM). The formulation of long-acting ocular drug delivery systems has been significantly advanced recently, with various LAR strategies developed for treatment of chronic ocular diseases [65–68]. Local intra-articular injections of mAbs in the knee have also been studied for treatment of osteoarthritis in a similar manner as local delivery anti-inflammatory agents and hyaluronic acid [69,70]. Collectively, these studies demonstrate an unmet need and significant opportunity to develop generalizable approaches for sustained, local release of mAbs and/or their fragments.

Biodegradable polymers are commonly desired because of difficulties associated with implantation and removal of nondegradable devices. For example, the new 6-month refillable Port Delivery System for release of the anti-vascular endothelial growth factor (anti-VEGF) Fab ranibizumab has encountered significant adverse events associated with the implantation of the device [71]. However, as described above, mAbs as proteins are often unstable when encapsulated and slowly

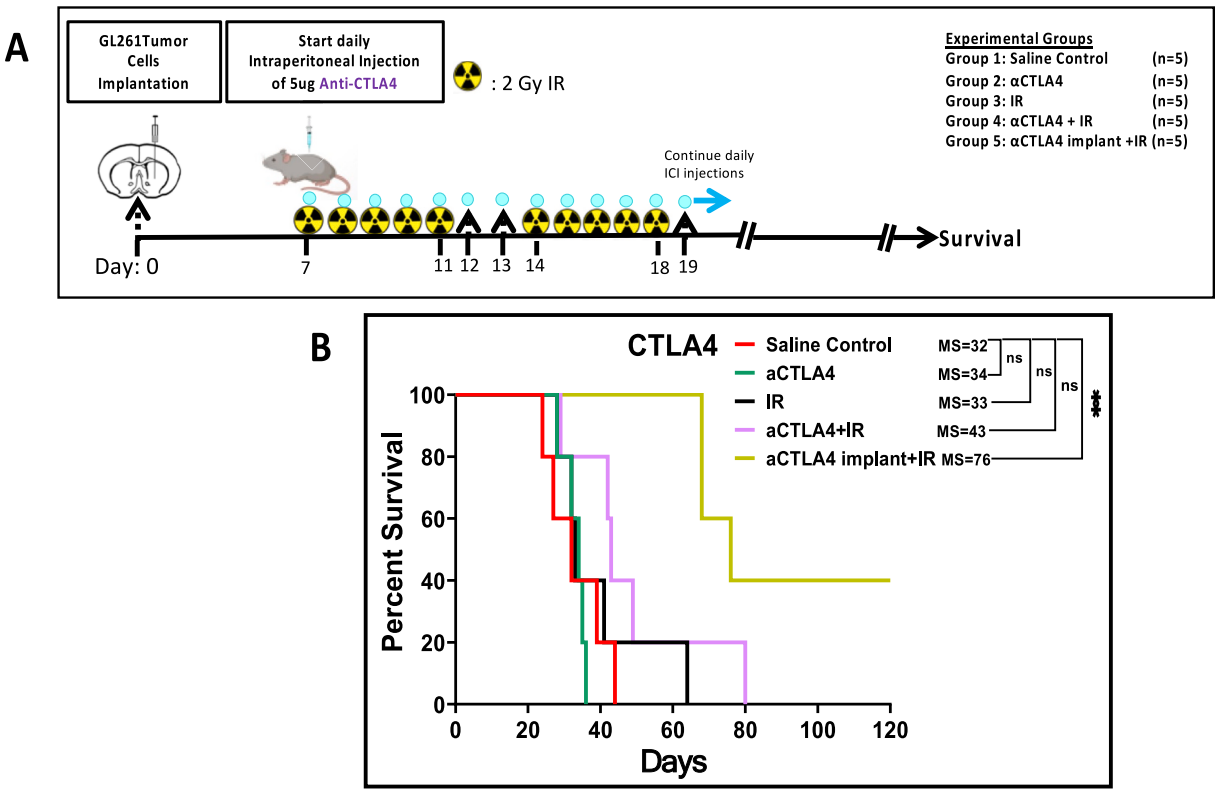

Fig. 6. Intratumoral CTLA-4 neutralization treatment in combination with radiation enhances survival of GBM-bearing mice. (A) Outline of treatment schedule of mice with GL261 tumors treated with saline, anti-CTLA-4, IR and anti-CTLA-4 implant on day 7 and administered 2 Gy/day for 10 days. (B) Kaplan-Meier survival analysis of GL261 tumor-bearing animals treated with saline, anti-CTLA-4, IR, anti-CTLA-4 + IR, anti-CTLA-4 implants+IR. Data were analyzed using the log-rank (Mantel-Cox) test. $^{**}p < 0.01$. MS indicates median survival in days.

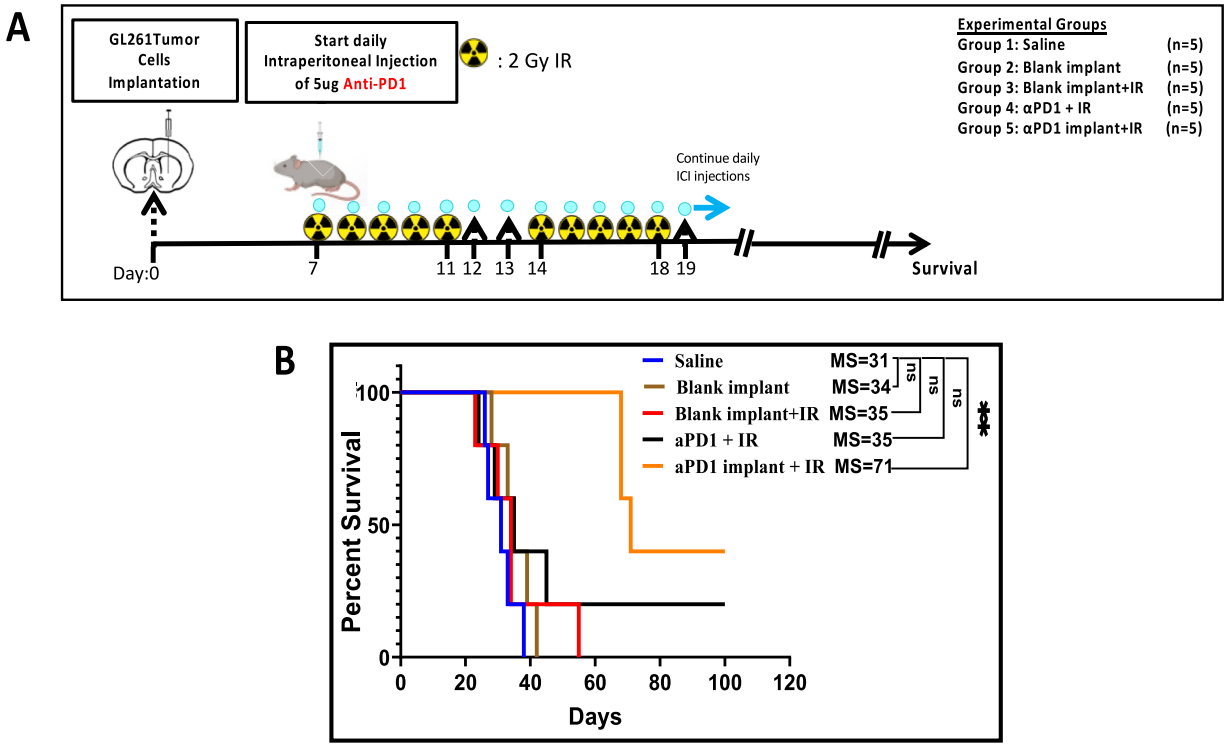

Fig. 7. Immune checkpoint blockade inhibitor (anti-PD-1) treatment of GBM-bearing mice in combination with radiation increases survival (A) Outline of treatment schedule of mice with GL261 tumors treated with saline, Blank Implant, Blank implant+IR, anti-PD-1 + IR and anti-PD-1 implant +IR on day 7 along with 2 Gy/day of irradiation for 10 days. (B) Kaplan-Meier survival analysis of GL261 tumor-bearing animals treated with saline, Blank Implant, Blank implant+IR, anti-PD-1 + IR, anti-PD-1 implant+ IR. Data were analyzed using the log-rank (Mantel-Cox) test. $^{**}p < 0.01$. MS indicates median survival in days.

released from biodegradable polymers [31]. The generalizable strategy for slow and continuous release of stable mAbs from PLGA similarly as described here with key improvements where necessary (e.g., smaller size, longevity, and more extensive stability analysis) could fill an unmet need for slow release of mAbs and potentially their fragments (e.g., Fabs and nanobodies) in the future.

4.2. VEGF inhibition for treatment of wet AMD

Local administration of anti-VEGF mAbs and related biologics has had a remarkable influence on wet AMD treatment [72]. This treatment is now an approved therapy for diabetic retinopathy, diabetic macular edema, macular edema following retinal vein occlusion and myopic choroidal neovascularization [9,73]. The presence of the vitreous provides significant longevity for a few weeks after administration as indicated by the strong reduction in half-life after vitrectomy [61]. However, a considerable portion of wet AMD patients do not comply adequately with the AMD treatment and follow-up protocol. The most frequent reasons for non-compliance with the required protocol are fear of intravitreal injection, subjective dissatisfaction with the benefit of the treatment, and financial limitations and difficulty in travel to and from the hospital [13,74]. Options to extend duration of anti-VEGF therapy include an Encapsulated Cell Technology (ECT) producing anti-VEGF proteins in the vitreous (NT-503), a Posterior MicroPump (PMP) delivery system, abicipar pegol (DARPin® based anti-angiogenic drug), and brolucizumab (anti-VEGF chain antibody fragment) [75]. The NT-503 ECT implant is based on the engineered cell line, which continuously produces a soluble VEGF receptor fusion protein. Despite its potential of long-acting anti-VEGF efficacy, the phase 2 clinical trial was discontinued due to a larger than anticipated number of treated patients requiring rescue medication [76,77]. The PMP for sustained delivery of anti-VEGF drugs has successfully completed first-in-man safety study [78]. However, this large size system requires surgical implantation on the sclera, which could be a significant burden for patients and physicians. Both abicipar and brolucizumab, which are new-class anti-VEGF drugs, have recently resulted in successful outcomes with 12-week dosing intervals in their phase 3 clinical trials [75,79].

Among long-term controlled release treatments, the FDA approved Port Delivery System with ranibizumab (PDS), as described above, is a small, refillable device, slightly longer than a grain of rice, surgically implanted in the eye and uniquely designed to continuously deliver ranibizumab which can be refilled through the subconjunctival port in the office as needed [9]. Widespread use of this new device has not yet taken place, likely due to some adverse reactions, particularly upon insertion [80]. A biodegradable device based on a nanoporous poly (caprolactone) (PCL) thin-film is also of interest, however, such a device is substantially large (~10 mm) and the slow biodegradation of PCL would result in significant buildup of polymer during chronic therapy [39].

4.3. Controlled release of bevacizumab from coated PLGA implants

Anhydrous encapsulation, optimization of the mAb loading, level of stabilizing excipient (trehalose), presence of a basic additive ($MgCO_3$), and concentration of PLGA coating over core implant were all critical for an ideal encapsulation and continuous release of stable mAb for >6–8 weeks with a low initial burst release. The stabilizing excipient, trehalose, was necessary in order to maintain stability and prevent aggregation of mAb during formulation, but with high levels of trehalose or with high loading of mAb (>10 %), release significantly increased due to high levels of water-soluble components and the resulting osmotic pressure inside the implant. Desirable features of mAb controlled release formulations include a high antibody loading, low initial burst release, a total cumulative release >80 %, and slow and continuous release for >6–12 weeks in vitro and in vivo. Furthermore, it is crucial to stabilize the mAb during processing and up until it is released in order to eliminate potential adverse reactions and to deliver therapeutically active antibody. Thus, proper evaluation of stability and activity is necessary after encapsulation and throughout the release period, particularly as it relates to soluble and insoluble protein aggregation.

Many past formulation approaches for controlled release of mAbs from biodegradable polymers are satisfactory in one or more of the critical delivery aspects described above, but not in combination, and have only been applied to 1–2 antibodies [32–46,81,82]. Key challenges to deliver mAbs include stabilization of the protein during encapsulation and release for extended periods while at the same time providing slow and continuous mAb release. We have previously demonstrated [50,51,83] for several proteins such as albumin, basic fibroblast growth factor, and tissue plasminogen activator, a technique that combines (a) mild microencapsulation conditions by anhydrous solvent extrusion into silicone rubber tubing to avoid protein denaturation under high shear, high temperature and/or organic solvent exposure [50,51,83–89] and (b) a combination of elevated protein loading (~15 % *w*/w) and suitable level of poorly soluble base (~3 % w/w $Mg(OH)_2$ or $MgCO_3$) in an end-capped PLGA 50/50 of moderate MW to avoid strong protein/PLGA interactions and large drops in microclimate pH, and to provide continuous protein release after an acceptable initial burst.

Starting from this formulation proven for a number of proteins, when encapsulating the mAb, bevacizumab, we encountered the additional issue of protein damage during micronization of the protein (Supplementary Fig. 2). We added the important stabilizer, trehalose, as is included in the commercial Avastin® solution formulation, to the dry powder at an optimal level to both stabilize bevacizumab during micronization and to minimize osmotic pressure (primarily from trehalose) and total water-soluble solid level (from trehalose + mAb) in the implant. By applying a unique PLGA coating over the core implant, the resulting osmotic pressure induced by the elevated trehalose and the percolation of water-soluble solids was controlled to allow the slow release to occur. The developed strategy was successful for 5 different mAbs to deliver completely an efficacious high dose of stabilized and immuno/bioreactive mAb in vitro and in vivo with continuous release properties and low initial burst release that has yet to be achieved from desirable PLGA, most commonly used in PLGA depots [90]. The continuous release kinetics likely occurs both through the uncoated rod ends and the coated lateral surface. Diffusional and osmotically induced release of mAb as the PLGA slowly erodes can be rationalized by the well-known steady pore-formation expected (at ends and lateral surface) and observed along the lateral surface of the coating in Supplementary Fig. 6, as a result of the slow conversion of co-encapsulated $MgCO_3$ to Mg-carboxylate salts and/or CO_2 upon polymer erosion and the osmotic pressure resulting from the high trehalose content [91].

Implants loaded with 400 μg of bevacizumab were evaluated in two intravitreal rabbit models, (i) the DL-AAA model which represents chronic induced leakage, and (ii) in healthy rabbits challenged with exogenous VEGF challenge after treatment. In both models, the bevacizumab implants outperformed the free mAb control group in retinal leakage protection. Since the rabbit body temperature [92] is higher than humans, implant performance would be expected to even improve in humans due to the lower thermal stress on the mAb. An initial in vivo biocompatibility study was performed to ensure the safety of the intravitreal implants in healthy rabbits. Histological findings described above were infrequent and suggestive of localized retinal or lenticular impaction only in 2 animals and expected mild macrophagic response to implant degradation, which was likely caused by the size of the implant in the relatively small rabbit eye. It is important to remark that immunogenicity, one of the key attributes of antibody products, has not been evaluated in this study. However, the significantly improved cumulative release (~89 %) and low residual aggregation of antibody (~9 % with ~98 % total mAb recovery) of the coated implant (Supplementary Table 9) together with the biocompatibility data collectively demonstrate the potential for favorable immunogenicity. To translate this or next generation implants formulation into clinical development, thorough

evaluation of immunogenicity and possible further adjustment of stabilizing parameters to further minimize residual, and non-releasable aggregated, protein and potential immunogenicity would be necessary. In the coated PLGA system described here, the cylinders will likely need to be smaller for ocular applications. At 0.8–0.9 mm diameter, they are currently slightly larger than the desired diameter for intravitreal injections (e.g., 0.46 mm of Ozurdex® implant [93]) and may require attention to PLGA-induced inflammation (e.g., addition of anti-inflammatory controlled release segments [43,49] or further lactic/glycolic acid neutralization by antacid excipients [51]. This size limitation, however, is not expected to be so limiting for a number of other local delivery applications, and the anti-VEGF coated implants developed here may have applications both with peri-tumoral edema associated with cancer of the brain [94] and arthritis of the knee [69] without further size reduction.

It is important to note that other interesting reports of mAb encapsulation and polymer delivery have been performed [32–46,81,82], although not with all of the benchmarks achieved here (high protein loading, low initial burst, continuous and virtually complete release >30 days, high stability of released protein (SEC, CD, ELISA, bioactivity), low insoluble aggregation, excellent initial biocompatibility, and positive in vivo efficacy). For example, one study [35] encapsulated two mAbs useful for cancer treatment (anti-CD40 and anti-CTLA4) in PLGA-like microspheres prepared from poly(hydroxymethyllactic-*co*-glycolic acid), known for being less susceptible to an acidic pH in the polymer [81]. The microspheres prepared by the deleterious double-emulsion method possessed a low drug loading (<1 % or less). Quantifying the mAbs by intrinsic fluorescence in vitro a 24-h initial burst of >40 % was reported with slow release over 28 days thereafter. No stability indicating assays (e.g., SEC, ELISA, CD, bioactivity) were used. In another promising study [82], an anti-TNF-a mAb was spray dried in the presence of lower levels of trehalose and histidine before encapsulating the protein powder in PLGA microspheres by a solid-in-oil-in-water method at elevated theoretical loading (~17.4 %) without further pH modifying excipients. MAb loading determined by a liquid-liquid extraction was high at 12–13 % *w*/w (~69–75 % EE). For PLGA 50/50 microspheres, most of the mAb was slowly released after a modest initial burst as recorded by UV spectroscopy over 28 days with significant fragmentation (7.1 %) by SEC. High immunoreactivity (83–100 %) and modest bioactivity (~46–64 %) was observed relative to the concentration from the absorbance values over the release interval. No direct protein structural and insoluble aggregation data, or in vivo experimentation were reported. Note that we have shown that encapsulation in aliphatic ester-end-capped PLGA 50/50 millirods or microspheres at high protein loading and in the absence of pH-modifying species both protein fragmentation and insoluble aggregation is common with model proteins such as albumin, owing to a lowering of pH and ensuing protein unfolding and peptide-bond hydrolysis [51]. We in contrast did not observe significant fragmentation in our SEC chromatograms. Therefore, the formulations in the above latter study and other formulations applying PLGA for mAb delivery without a pH-modifying strategy are expected to significantly damage the encapsulated protein during release incubation by the well-established acidification of the microclimate in the polymer.

4.4. Immune checkpoint inhibitor immunotherapy for treatment of GBM

The current standard-of-care for GBM, consisting of surgical resection, radiotherapy, and chemotherapy, results in a median survival of 14 to 20 months in humans. Only 5 % of patients survive approximately 5 years making GBM one of the most deadly primary tumors [95]. GBM has a high incidence of recurrence and evades the immune system through the upregulation of immune checkpoint inhibitors, such as PD-1/PD-L1, contributing to its high recurrence rate [18,95]. Anti-PD-1 and anti-CTLA-4 are both in phase 1 clinical trials for GBM (NCT04606316), but suffer from systemic-related toxicity that can result in cessation of treatment [20]. Delivering immune checkpoint inhibitors locally through sustained release implants could potentially benefit GBM treatment by avoiding systemic toxicity and extending antibody presence at the tumor site [22].

4.5. Controlled release of anti-PD-1 and anti-CTLA-4 from coated PLGA implants

Adapting the optimized implant formulation of bevacizumab by adding a second PLGA coating over the core implant reduced the initial burst. Anti-PD-1 and anti-CTLA-4 implants released mAb continuously for >6 weeks with maintained secondary structure and low losses of monomeric content and immunoreactivity/bioactivity. Implants were evaluated in combination with radiation therapy in a GBM murine model and were effective at mitigating disease progression and increasing immunological memory. The results showed that combining the anti-PD-1 and anti-CTLA-4 controlled release implants with radiation, extended the median survival (MS) significantly. In the anti-CTLA-4 implant group, median survival increased from 32 days (Saline control) to 76 days. In the anti-PD-1 implant group, it increased from 28 days (saline control) to 71 days. The combination of free antibodies given intraperitoneally with radiation did not result in a significant change in median survival (MS), with MS of 35 days for free anti-PD-1 + IR and 43 days for free anti-CTLA-4 + IR. The specific mechanisms underlying the differences in therapeutic effects among various treatment regimens remain unclear and require further investigation, such as through flow cytometry or MRI imaging.

The implantable sub-millimeter rod system described here is adaptable [83] to additional bioactive agents such as immune stimulators (e.g., CpG) [96,97] and tumor penetration-enhancing cytotoxic agents (e.g., docetaxel) [98,99]. Combination therapies offer increased survival in GBM over single arm therapies and both CpG and docetaxel are actively pursued options for GBM [98,100–103]. Therefore, by formulating PLGA implants for sustained release of the CpG and combining them with immune checkpoint inhibitor implants described here, we can anticipate a stronger and more effective immune response. Additionally, this approach can potentially be used to enhance tumor cell apoptosis and improve penetration using docetaxel, thereby increasing the overall therapeutic impact [101,104–106].

5. Conclusion and outlook

The potential for local controlled release mAbs from PLGA is highly significant. There are very few local delivery options for the best-selling drug class despite a well-known difficulty to access vital areas of the body by systemic administration, and with minimal side-effects. Our data clearly shows a broad potential of carefully formulated coated PLGA/trehalose/$MgCO_3$ implants to slowly and continuously release a variety of unrelated immunoreactive mAbs for >6–8 weeks with strong efficacy in two difficult-to-reach organs, the eye and brain. A judicious combination of past anhydrous PLGA encapsulation techniques [51,52,83], selection of stabilizing excipients (trehalose and $MgCO_3$), and novel coating to obviate the necessarily high osmotic pressure created within the implant, provides implants that contain elevated drug load (~6–8 % *w*/w) and degrade on a reasonable time-scale to avoid polymer build-up during repeated administrations. This formulation strategy could easily be envisioned to benefit local therapies for both existing mAb therapeutics and those mAbs under development or discarded because of systemic toxicity [20,64,107,108]. More research is necessary to realize the potential of this approach including: (a) further reduction in implant diameter to <0.5 mm to decrease intravitreal needle size for improved patient acceptability and reduced risk of adverse effects [109]; (b) further evaluation and management of mild PLGA-induced inflammation in sensitive tissues such as the eye, brain, and joint [110]; (c) the extent and necessity of tissue penetration [111–113] of immune checkpoint mAbs in brain tissues for GBM and

other local tumor therapies; (d) the selection of appropriate adjunct therapies (e.g., radiation [114], adjuvants [96,97], neoantigens [115], chemotherapy [98,99]) for optimization of the local immune checkpoint effect; and (e) further optimization of the polymer formulation to maximize activity and reduce residual protein aggregation at the end of the release period for certain mAbs. With such initiatives, the application of local controlled-release strategies for mAbs, such as presented here, could have a reasonable path to the clinic.

Authors contribution

S.P·S., D.A.A., M.G.C., and A.S. designed the project and S.P.S., J.W., R.S·C., M.G.C., and Y.H. wrote the manuscript. R.S.C. and S.P.S. developed bevacizumab implants and implant coating method. R.S.C. formulated bevacizumab implants and performed in vitro analyses with contribution from K.P. on circular dichroism. J.W. formulated anti-PD-1 and anti-CTLA-4 implants, with contribution from R.S.C, and performed in vitro analyses. P.K. and A.A.M. performed GBM in vivo experiments and analyses and J.J. performed in vivo experiments for the DL-AAA induced chronic leakage model and VEGF-induced leakage model. All authors analyzed and interpreted the data.

CRediT authorship contribution statement

Rae Sung Chang: Writing – original draft, Software, Methodology, Investigation, Formal analysis, Data curation. **Jennifer Walker:** Writing – original draft, Software, Methodology, Investigation, Formal analysis, Data curation. **Anzar A. Mujeeb:** Writing – original draft, Visualization, Methodology, Investigation, Formal analysis, Data curation. **Padma Kadiyala:** Visualization, Software, Methodology, Formal analysis, Data curation. **Karthik Pisupati:** Supervision, Methodology, Formal analysis, Data curation. **Jeffrey Jamison:** Visualization, Validation, Formal analysis, Data curation. **Anna Schwendeman:** Writing – original draft, Resources, Project administration, Methodology, Investigation, Conceptualization. **Yusuf Haggag:** Writing – original draft, Methodology, Formal analysis. **David A. Antonetti:** Validation, Supervision, Project administration, Methodology, Investigation, Data curation, Conceptualization. **Maria G. Castro:** Writing – original draft, Validation, Supervision, Resources, Project administration, Methodology, Investigation, Data curation, Conceptualization. **Steven P. Schwendeman:** Writing – original draft, Validation, Supervision, Project administration, Methodology, Data curation, Conceptualization.

Declaration of competing interest

The authors declare the following financial interests/personal relationships which may be considered as potential competing interests: Drs. Steven P. Schwendeman and Rae Sung Chang are listed inventors on related intellectual property owned by the University of Michigan.

Acknowledgements

This work was funded by two UM Biointerfaces Institute internal challenge grants, The UM BioInnovations in Brain Cancer Program, an Ara G. Paul Professorship to S.P.S, R01 CA227273, R01 NS122536, R01 NS122165 and R01 NS124167 and partial support for Jennifer Walker by the Cellular Biotechnology Training Program (T32-GM008353). Authors would like to acknowledge Dr. Josh Errickson of the University of Michigan CSCAR (Consulting for Statistics, Computing & Analytics Research) for his statistical analysis of the DL-AAA model data and Ingrid L. Bergin of the University of Michigan IVAC (In-Vivo Animal Core) of ULAM (Unit for Laboratory Animal Medicine) for her histological analyses. The authors are greatful to BMS for supplying the anti-PD-1 and anti-CTLA4 mAbs used in this paper.

Appendix A. Supplementary data

Supplementary data to this article can be found online at https://doi.org/10.1016/j.jconrel.2025.113743.

Data availability

Data will be made available on request.

References

[1] C.W. Lindsley, New 2017 Data and statistics for pharmaceutical products, ACS Chem. Neurosci. 9 (2018) 1518–1519.
[2] D.C. Roopenian, S. Akilesh, FcRn: the neonatal fc receptor comes of age, Nat. Rev. Immunol. 7 (2007) 715–725.
[3] J.Y. Ljubimova, T. Sun, L. Mashouf, A.V. Ljubimov, L.L. Israel, V.A. Ljubimov, V. Falahatian, E. Holler, Covalent nano delivery systems for selective imaging and treatment of brain tumors, Adv. Drug Deliv. Rev. 113 (2017) 177–200.
[4] K.-I. Hosoya, M. Tomi, M. Tachikawa, Strategies for therapy of retinal diseases using systemic drug delivery: relevance of transporters at the blood–retinal barrier, Expert Opin. Drug Deliv. 8 (2011) 1571–1587.
[5] A.V. Chappelow, P.K. Kaiser, Neovascular age-related macular degeneration: potential therapies, Drugs 68 (2008) 1029–1036.
[6] A.D. Kulkarni, B.D. Kuppermann, Wet age-related macular degeneration, Adv. Drug Deliv. Rev. 57 (2005) 1994–2009.
[7] E.P. Rakoczy, Gene-and Cell-Based Treatment Strategies for the Eye, Springer, Berlin, Heidelberg, Germany, 2015.
[8] B.A. Syed, J.B. Evans, L. Bielory, Wet AMD market, Nat. Rev. Drug Discov. 11 (2012) 827.
[9] Lucentis(R), (ranibizumab injection) [FDA package insert], Genentech, Inc, San Francisco, CA, 2014.
[10] Eylea(TM), (aflibercept) [FDA Package Insert], Regeneron Pharmaceuticals, Inc, Tarrytown, NY, 2011.
[11] M. Shirley, Faricimab: first approval, Drugs 82 (2022) 825–830.
[12] K. Ghasemi Falavarjani, Q. Nguyen, Adverse events and complications associated with intravitreal injection of anti-VEGF agents: a review of literature, Eye 27 (2013) 787–794.
[13] K.M. Droege, P.S. Muether, M.M. Hermann, A. Caramoy, U. Viebahn, B. Kirchhof, S. Fauser, Adherence to ranibizumab treatment for neovascular age-related macular degeneration in real life, Graefe's archive for, Clin. Experiment. Ophthalmol. 251 (2013) 1281–1284.
[14] H. Mu, Y. Wang, Y. Chu, Y. Jiang, H. Hua, L. Chu, K. Wang, A. Wang, W. Liu, Y. Li, Multivesicular liposomes for sustained release of bevacizumab in treating laser-induced choroidal neovascularization, Drug Deliv. 25 (2018) 1372–1383.
[15] J.G. Ghosh, A.A. Nguyen, C.E. Bigelow, S. Poor, Y. Qiu, N. Rangaswamy, R. Ornberg, B. Jackson, H. Mak, T. Ezell, Long-acting protein drugs for the treatment of ocular diseases, Nat. Commun. 8 (2017) 14837.
[16] P. Badiee, R. Varshochian, M. Rafiee-Tehrani, F. Abedin Dorkoosh, M. R. Khoshayand, R. Dinarvand, Ocular implant containing bevacizumab-loaded chitosan nanoparticles intended for choroidal neovascularization treatment, J. Biomed. Mater. Res. A 106 (2018) 2261–2271.
[17] S. Tanaka, D.N. Louis, W.T. Curry, T.T. Batchelor, J. Dietrich, Diagnostic and therapeutic avenues for glioblastoma: no longer a dead end?,, Nat. Rev. Clin. Oncol. 10 (2013) 14–26.
[18] P.R. Lowenstein, M.G. Castro, Evolutionary basis of a new gene-and immune-therapeutic approach for the treatment of malignant brain tumors: from mice to clinical trials for glioma patients, Clin. Immunol. 189 (2018) 43–51.
[19] L. Gately, S. McLachlan, A. Dowling, J. Philip, Life beyond a diagnosis of glioblastoma: a systematic review of the literature, J. Cancer Surviv. 11 (2017) 447–452.
[20] L. Spain, S. Diem, J. Larkin, Management of toxicities of immune checkpoint inhibitors, Cancer Treat. Rev. 44 (2016) 51–60.
[21] J.R. Brahmer, C. Lacchetti, B.J. Schneider, M.B. Atkins, K.J. Brassil, J.M. Caterino, I. Chau, M.S. Ernstoff, J.M. Gardner, P. Ginex, Management of immune-related adverse events in patients treated with immune checkpoint inhibitor therapy: American Society of Clinical Oncology clinical practice guideline, J. Clin. Oncol. 36 (2018) 1714–1768.
[22] R. Maxwell, C.M. Jackson, M. Lim, Clinical trials investigating immune checkpoint blockade in glioblastoma, Curr. Treat. Options Oncol. 18 (2017) 1–22.
[23] M. Lim, Y. Xia, C. Bettegowda, M. Weller, Current state of immunotherapy for glioblastoma,, Nat. Rev. Clin. Oncol. 15 (2018) 422–442.
[24] C.J. Bertens, M. Gijs, F.J. van den Biggelaar, R.M. Nuijts, Topical drug delivery devices: a review, Exp. Eye Res. 168 (2018) 149–160.
[25] F.J. Attenello, D. Mukherjee, G. Datoo, M.J. McGirt, E. Bohan, J.D. Weingart, A. Olivi, A. Quinones-Hinojosa, H. Brem, Use of Gliadel (BCNU) wafer in the surgical treatment of malignant glioma: a 10-year institutional experience, Ann. Surg. Oncol. 15 (2008) 2887–2893.
[26] I. Major, E. Fuenmayor, C. McConville, The production of solid dosage forms from non-degradable polymers, Curr. Pharm. Des. 22 (2016) 2738–2760.
[27] D.R. Friend, Intravaginal rings: controlled release systems for contraception and prevention of transmission of sexually transmitted infections, Drug Deliv. Transl. Res. 1 (2011) 185–193.

[28] K. Abdullah, B. Bou Dargham, M. Steinbrecher, B. Sun, Z. Huiqiang, H. Khalili, E. S. Brilakis, S. Banerjee, Drug-eluting stents for treatment of peripheral artery disease,, Am. J. Cardiovasc. Drugs 18 (2018) 175–180.
[29] W.A. Gray, K. Keirse, Y. Soga, A. Benko, A. Babaev, Y. Yokoi, H. Schroeder, J. T. Prem, A. Holden, J. Popma, A polymer-coated, paclitaxel-eluting stent (eluvia) versus a polymer-free, paclitaxel-coated stent (Zilver PTX) for endovascular femoropopliteal intervention (IMPERIAL): a randomised, non-inferiority trial, Lancet 392 (2018) 1541–1551.
[30] N. Bodick, J. Lufkin, C. Willwerth, A. Kumar, J. Bolognese, C. Schoonmaker, R. Ballal, D. Hunter, M. Clayman, An intra-articular, extended-release formulation of triamcinolone acetonide prolongs and amplifies analgesic effect in patients with osteoarthritis of the knee: a randomized clinical trial, JBJS 97 (2015) 877–888.
[31] M. van de Weert, W.E. Hennink, W. Jiskoot, Protein instability in poly (lactic-co-glycolic acid) microparticles, Pharm. Res. 17 (2000) 1159–1167.
[32] M.D. Baumann, C.E. Kang, J.C. Stanwick, Y. Wang, H. Kim, Y. Lapitsky, M. S. Shoichet, An injectable drug delivery platform for sustained combination therapy, J. Control. Release 138 (2009) 205–213.
[33] J.C. Stanwick, M.D. Baumann, M.S. Shoichet, In vitro sustained release of bioactive anti-NogoA, a molecule in clinical development for treatment of spinal cord injury, Int. J. Pharm. 426 (2012) 284–290.
[34] J. Wang, K.M. Chua, C.-H. Wang, Stabilization and encapsulation of human immunoglobulin G into biodegradable microspheres, J. Colloid Interface Sci. 271 (2004) 92–101.
[35] S. Rahimian, M.F. Fransen, J.W. Kleinovink, M. Amidi, F. Ossendorp, W. E. Hennink, Polymeric microparticles for sustained and local delivery of antiCD40 and antiCTLA-4 in immunotherapy of cancer, Biomaterials 61 (2015) 33–40.
[36] S. Koutsopoulos, S. Zhang, Two-layered injectable self-assembling peptide scaffold hydrogels for long-term sustained release of human antibodies, J. Control. Release 160 (2012) 451–458.
[37] J. Mordenti, K. Thomsen, V. Licko, L. Berleau, J.W. Kahn, R.A. Cuthbertson, E. T. Duenas, A.M. Ryan, C. Schofield, T.W. Berger, Y.G. Meng, J. Cleland, Intraocular pharmacokinetics and safety of a humanized monoclonal antibody in rabbits after intravitreal administration of a solution or a PLGA microsphere formulation, Toxicol. Sci. 52 (1999) 101–106.
[38] F. Li, B. Hurley, Y. Liu, B. Leonard, M. Griffith, Controlled release of bevacizumab through nanospheres for extended treatment of age-related macular degeneration, Open Ophthalmol. J. 6 (2012) 54–58.
[39] K.D. Lance, D.A. Bernards, N.A. Ciaccio, S.D. Good, T.S. Mendes, M. Kudisch, E. Chan, M. Ishikiriyama, R.B. Bhisitkul, T.A. Desai, In vivo and in vitro sustained release of ranibizumab from a nanoporous thin-film device,, Drug Deliv. Transl. Res. 6 (2016) 771–780.
[40] W.M. Tian, C.L. Zhang, S.P. Hou, X. Yu, F.Z. Cui, Q.Y. Xu, S.L. Sheng, H. Cui, H. D. Li, Hyaluronic acid hydrogel as Nogo-66 receptor antibody delivery system for the repairing of injured rat brain: in vitro, J. Controlled Release 102 (2005) 13–22.
[41] J.S. Andrew, E.J. Anglin, E.C. Wu, M.Y. Chen, L. Cheng, W.R. Freeman, M. J. Sailor, Sustained release of a monoclonal antibody from electrochemically prepared mesoporous silicon oxide, Adv. Funct. Mater. 20 (2010) 4168–4174.
[42] D. Schweizer, K. Schönhammer, M. Jahn, A. Göpferich, Protein-polyanion interactions for the controlled release of monoclonal antibodies, Biomacromolecules 14 (2013) 75–83.
[43] A. Cossé, C. König, A. Lamprecht, K.G. Wagner, Hot melt extrusion for sustained protein release: matrix erosion and in vitro release of PLGA-based implants, AAPS PharmSciTech 18 (2017) 15–26.
[44] P. Adamson, T. Wilde, E. Dobrzynski, C. Sychterz, R. Polsky, E. Kurali, R. Haworth, C.M. Tang, J. Korczynska, F. Cook, I. Papanicolaou, L. Tsikna, C. Roberts, Z. Hughes-Thomas, J. Walford, D. Gibson, J. Warrack, J. Smal, R. Verrijk, P.E. Miller, T.M. Nork, J. Prusakiewicz, T. Streit, S. Sorden, C. Struble, B. Christian, I.R. Catchpole, Single ocular injection of a sustained-release anti-VEGF delivers 6 months pharmacokinetics and efficacy in a primate laser CNV model, J. Controlled Release 244 (2016) 1–13.
[45] P. Tyagi, M. Barros, J.W. Stansbury, U.B. Kompella, Light-activated, in situ forming gel for sustained suprachoroidal delivery of bevacizumab, Mol. Pharm. 10 (2013) 2858–2867.
[46] M. Gregoritza, V. Messmann, K. Abstiens, F.P. Brandl, A.M. Goepferich, Controlled antibody release from degradable Thermoresponsive hydrogels cross-linked by Diels-Alder chemistry, Biomacromolecules 18 (2017) 2410–2418.
[47] F. Sousa, A. Cruz, I.M. Pinto, B. Sarmento, Nanoparticles provide long-term stability of bevacizumab preserving its antiangiogenic activity, Acta Biomater. 78 (2018) 285–295.
[48] S.A. Giannos, E.R. Kraft, Z.Y. Zhao, K.H. Merkley, J. Cai, Formulation stabilization and disaggregation of bevacizumab, ranibizumab and aflibercept in dilute solutions, Pharm. Res. 35 (2018) 78.
[49] Ozurdex(R), [FDA Package Insert], Irvine, CA, Allergan, 2014.
[50] G. Zhu, S.P. Schwendeman, Stabilization of proteins encapsulated in cylindrical poly(lactide-co-glycolide) implants: mechanism of stabilization by basic additives, Pharm. Res. 17 (2000) 351–357.
[51] G. Zhu, S.R. Mallery, S.P. Schwendeman, Stabilization of proteins encapsulated in injectable poly (lactide- co-glycolide), Nat. Biotechnol. 18 (2000) 52–57.
[52] Y. Zhong, L. Zhang, A.G. Ding, A. Shenderova, G. Zhu, P. Pei, R.R. Chen, S. R. Mallery, D.J. Mooney, S.P. Schwendeman, Rescue of SCID murine ischemic hindlimbs with pH-modified rhbFGF/poly(DL-lactic-co-glycolic acid) implants, J. Controlled Release 122 (2007) 331–337.
[53] Y. Li, J.M. Busoy, B.A.A. Zaman, Q.S.W. Tan, G.S.W. Tan, V.A. Barathi, N. Cheung, J.J. Wei, W. Hunziker, W. Hong, T.Y. Wong, C.M.G. Cheung, A novel model of persistent retinal neovascularization for the development of sustained anti-VEGF therapies, Exp. Eye Res. 174 (2018) 98–106.
[54] J. Cao, T.C. MacPherson, B.V. Iglesias, Y. Liu, N. Tirko, G.D. Yancopoulos, S. J. Wiegand, C. Romano, Aflibercept action in a rabbit model of chronic retinal neovascularization: reversible inhibition of pathologic leakage with dose-dependent duration, Invest. Ophthalmol. Vis. Sci. 59 (2018) 1033–1044.
[55] R.M. Murillo, A. Martinez, Animal Models of Brain Tumors, Humana Totowa, NJ, 2013.
[56] AVASTIN®. (bevacizumab), labeling text, Label Amend, 2009, pp. 1–22.
[57] E.M. Moussa, J.P. Panchal, B.S. Moorthy, J.S. Blum, M.K. Joubert, L.O. Narhi, E. M. Topp, Immunogenicity of therapeutic protein aggregates, J. Pharm. Sci. 105 (2016) 417–430.
[58] N.K. Jain, I. Roy, Effect of trehalose on protein structure, Protein Sci. 18 (2009) 24–36.
[59] N.K. Jain, I. Roy, Trehalose and Protein Stability, Current Protocols in Protein Science, John Wiley & Sons, Ltd, Chichester, UK, 2010, pp. 4–9.
[60] S.J. Bakri, M.R. Snyder, J.M. Reid, J.S. Pulido, R.J. Singh, Pharmacokinetics of intravitreal bevacizumab (Avastin), Ophthalmology 114 (2007) 855–859.
[61] E. Moisseiev, M. Waisbourd, E. Ben-Artsi, E. Levinger, A. Barak, T. Daniels, K. Csaky, A. Loewenstein, I.S. Barequet, Pharmacokinetics of bevacizumab after topical and intravitreal administration in human eyes, Graefes Arch. Clin. Exp. Ophthalmol. 252 (2014) 331–337.
[62] FDA, Oncologic Drugs Advisory Committee, Opdivo/Nivolumab Label, 2015.
[63] Yervoy(R), (ipilimumab), [FDA Package Insert], Bristol-Myers Squibb Company, Princeton, NJ, 2011.
[64] M.A. Postow, R. Sidlow, M.D. Hellmann, Immune-related adverse events associated with immune checkpoint blockade, N. Engl. J. Med. 378 (2018) 158–168.
[65] D. Waite, F.M. Adrianto, F. Annuyanti, Y. So, W. Zhang, S. Wang, Y. Wu, Y. Wang, T. Raghu Raj Singh, 3 - long-acting drug delivery systems for ocular therapies, in: E. Larrañeta, T. Raghu Raj Singh, R.F. Donnelly (Eds.), Long-Acting Drug Delivery Systems, Woodhead Publishing, 2022, pp. 61–81.
[66] M.N. O'Brien Laramy, K. Nagapudi, Long-acting ocular drug delivery technologies with clinical precedent, Expert Opin. Drug Deliv. 19 (2022) 1285–1301.
[67] M. Mostafa, A. Al Fatease, R.G. Alany, H. Abdelkader, Recent advances of ocular drug delivery systems: prominence of ocular implants for chronic eye diseases, Pharmaceutics 15 (2023) 1746.
[68] Y.Y. Cong, B. Fan, Z.Y. Zhang, G.Y. Li, Implantable sustained-release drug delivery systems: a revolution for ocular therapeutics, Int. Ophthalmol. 43 (2023) 2575–2588.
[69] W. Li, J. Lin, Z. Wang, S. Ren, X. Wu, F. Yu, J. Weng, H. Zeng, Bevacizumab tested for treatment of knee osteoarthritis via inhibition of synovial vascular hyperplasia in rabbits, J. Orthopaedic Transl. 19 (2019) 38–46.
[70] T. Nagai, M. Sato, M. Kobayashi, M. Yokoyama, Y. Tani, J. Mochida, Bevacizumab, an anti-vascular endothelial growth factor antibody, inhibits osteoarthritis, Arthritis Res. Ther. 16 (2014) 427.
[71] S.J. Lowater, J. Grauslund, Y. Subhi, A.S. Vergmann, Clinical trials and future outlooks of the port delivery system with Ranibizumab: a narrative review, Ophthalmol Therapy 13 (2024) 51–69.
[72] J.L. Kovach, S.G. Schwartz, H.W. Flynn Jr., I.U. Scott, Anti-VEGF treatment strategies for wet AMD, J. Ophthalmol. 2012 (2012) 786870.
[73] S.H. Shahcheraghi, A.A.A. Aljabali, M.S. Al Zoubi, V. Mishra, N.B. Charbe, Y. A. Haggag, G. Shrivastava, A.G. Almutary, A.M. Alnuqaydan, D. Barh, K. Dua, D. K. Chellappan, G. Gupta, M. Lotfi, Á. Serrano-Aroca, B. Bahar, Y.K. Mishra, K. Takayama, P.K. Panda, H.A. Bakshi, M.M. Tambuwala, Overview of key molecular and pharmacological targets for diabetes and associated diseases, Life Sci. 278 (2021) 119632.
[74] O. Polat, S. İnan, S. Özcan, M. Doğan, T. Küsbeci, G.F. Yavaş, Ü. İnan, Factors affecting compliance to intravitreal anti-vascular endothelial growth factor therapy in patients with age-related macular degeneration, Turkish, J. Ophthalmol. 47 (2017) 205–210.
[75] M.W. Stewart, Extended duration vascular endothelial growth factor inhibition in the eye: failures, successes, and future possibilities, Pharmaceutics 10 (2018) 21.
[76] H. Chen, Recent developments in ocular drug delivery, J. Drug Target. 23 (2015) 597–604.
[77] A. Loewenstein, H. Quiroz-Mercado, J.L. Guerrero-Naranjo, S. Rojas, A. Santos, J. C. Altamirano, Y. Morales, R. Schiffman, Interim results of a dose escalation study of NT-503 encapsulated cell therapy for the treatment of choroidal neovascularization in AMD, Invest. Ophthalmol. Vis. Sci. 56 (2015) 2277.
[78] J.C. Gutiérrez-Hernández, S. Caffey, W. Abdallah, P. Calvillo, R. González, J. Shih, J. Brennan, J. Zimmerman, J.C. Martínez-Camarillo, A.R. Rodriguez, R. Varma, A. Santos, G. Sánchez, M. Humayun, One-year feasibility study of replenish MicroPump for intravitreal drug delivery: a pilot study, Transl. Vis. Sci. Technol. 3 (2014) 8.
[79] P.U. Dugel, A. Koh, Y. Ogura, G.J. Jaffe, U. Schmidt-Erfurth, D.M. Brown, A. V. Gomes, J. Warburton, A. Weichselberger, F.G. Holz, HAWK and HARRIER: phase 3, multicenter, randomized, double-masked trials of brolucizumab for neovascular age-related macular degeneration, Ophthalmology 127 (2020) 72–84.
[80] N.M. Holekamp, P.A. Campochiaro, M.A. Chang, D. Miller, D. Pieramici, A. P. Adamis, C. Brittain, E. Evans, D. Kaufman, K.F. Maass, S. Patel, S. Ranade, N. Singh, G. Barteselli, C. Regillo, Archway randomized phase 3 trial of the port delivery system with ranibizumab for neovascular age-related macular degeneration, Ophthalmology 129 (2022) 295–307.

[81] Y. Liu, A.H. Ghassemi, W.E. Hennink, S.P. Schwendeman, The microclimate pH in poly(D,L-lactide-co-hydroxymethyl glycolide) microspheres during biodegradation, Biomaterials 33 (2012) 7584–7593.
[82] S. Marquette, C. Peerboom, A. Yates, L. Denis, I. Langer, K. Amighi, J. Goole, Stability study of full-length antibody (anti-TNF alpha) loaded PLGA microspheres, Int. J. Pharm. 470 (2014) 41–50.
[83] T. Zhou, H. Lewis, R.E. Foster, S.P. Schwendeman, Development of a multiple-drug delivery implant for intraocular management of proliferative vitreoretinopathy, J. Control. Release 55 (1998) 281–295.
[84] S.P. Schwendeman, M. Cardamone, M.R. Brandon, A.M. Klibanov, R. Langer, Stability of proteins and their delivery from biodegradable polymer microspheres, in: S. Cohen, H. Bernstein (Eds.), Microparticulate Systems for the Delivery of Proteins and Vaccines, 1st Edition, Marcel Dekker, 1996, pp. 1–49.
[85] S.E. Reinhold, K.G. Desai, L. Zhang, K.F. Olsen, S.P. Schwendeman, Self-healing microencapsulation of biomacromolecules without organic solvents, Angew. Chem. Int. Ed. Eng. 51 (2012) 10800–10803.
[86] K.G. Desai, S.R. Mallery, S.P. Schwendeman, Formulation and characterization of injectable poly(DL-lactide-co-glycolide) implants loaded with N-acetylcysteine, a MMP inhibitor, Pharm. Res. 25 (2008) 586–597.
[87] M. El-Tanani, A. Platt-Higgins, Y.-F. Lee, A.O. Al Khatib, Y. Haggag, M. Sutherland, S.-D. Zhang, A.A.A. Aljabali, V. Mishra, Á. Serrano-Aroca, M. M. Tambuwala, P.S. Rudland, Matrix metalloproteinase 2 is a target of the RAN-GTP pathway and mediates migration, invasion and metastasis in human breast cancer, Life Sci. 310 (2022) 121046.
[88] J. Kang, S.P. Schwendeman, Comparison of the effects of $Mg(OH)_2$ and sucrose on the stability of bovine serum albumin encapsulated in injectable poly(D,L-lactide-co-glycolide) implants, Biomaterials 23 (2002) 239–245.
[89] K.G. Desai, S.R. Mallery, S.P. Schwendeman, Effect of formulation parameters on 2-methoxyestradiol release from injectable cylindrical poly(DL-lactide-co-glycolide) implants, Eur. J. Pharmaceut. Biopharmaceut. 70 (2008) 187–198.
[90] H. Zhong, G. Chan, Y. Hu, H. Hu, D. Ouyang, A comprehensive map of FDA-approved pharmaceutical products, Pharmaceutics 10 (2018) 263.
[91] S.P. Schwendeman, R.B. Shah, B.A. Bailey, A.S. Schwendeman, Injectable controlled release depots for large molecules, J. Control. Release 190 (2014) 240–253.
[92] J. Mayer, Management of Rabbits, in: Merck Veterinary Manual, 2021.
[93] N. Yesilirmak, E.S. Ozdemir, D.D. Altinors, Effect of dexamethasone intravitreal implant in a corneal graft rejection, international, J. Ophthalmol. 9 (2016) 475–477.
[94] X. Meng, R. Zhao, G. Shen, D. Dong, L. Ding, S. Wu, Efficacy and safety of bevacizumab treatment for refractory brain edema: case report, Medicine 96 (2017) e8280.
[95] A. Omuro, L.M. DeAngelis, Glioblastoma and other malignant gliomas: a clinical review, JAMA 310 (2013) 1842–1850.
[96] A.M. Krieg, Antitumor applications of stimulating toll-like receptor 9 with CpG oligodeoxynucleotides, Curr. Oncol. Rep. 6 (2004) 88–95.
[97] A.F. Carpentier, G. Auf, J.Y. Delattre, CpG-oligonucleotides for cancer immunotherapy : review of the literature and potential applications in malignant glioma, Front. Biosci. 8 (2003) e115–e127.
[98] G. Lollo, M. Vincent, G. Ullio-Gamboa, L. Lemaire, F. Franconi, D. Couez, J. P. Benoit, Development of multifunctional lipid nanocapsules for the co-delivery of paclitaxel and CpG-ODN in the treatment of glioblastoma, Int. J. Pharm. 495 (2015) 972–980.
[99] M.G. Castro, R. Cowen, I.K. Williamson, A. David, M.J. Jimenez-Dalmaroni, X. Yuan, A. Bigliari, J.C. Williams, J. Hu, P.R. Lowenstein, Current and future strategies for the treatment of malignant brain tumors, Pharmacol. Ther. 98 (2003) 71–108.
[100] M.G. Castro, G.J. Baker, P.R. Lowenstein, Blocking immunosuppressive checkpoints for glioma therapy: the more the merrier!, Clin. Cancer Res 20 (2014) 5147–5149.
[101] A.F. Carpentier, J. Xie, K. Mokhtari, J.Y. Delattre, Successful treatment of intracranial gliomas in rat by oligodeoxynucleotides containing CpG motifs, Clin. Cancer Res. 6 (2000) 2469–2473.
[102] A. El Andaloussi, A.M. Sonabend, Y. Han, M.S. Lesniak, Stimulation of TLR9 with CpG ODN enhances apoptosis of glioma and prolongs the survival of mice with experimental brain tumors, Glia 54 (2006) 526–535.
[103] P. Kadiyala, D. Li, F.M. Nuñez, D. Altshuler, R. Doherty, R. Kuai, M. Yu, N. Kamran, M. Edwards, J.J. Moon, P.R. Lowenstein, M.G. Castro, A. Schwendeman, High-density lipoprotein-mimicking Nanodiscs for chemo-immunotherapy against glioblastoma Multiforme, ACS Nano 13 (2019) 1365–1384.
[104] S.H. Jang, M.G. Wientjes, D. Lu, J.L. Au, Drug delivery and transport to solid tumors, Pharm. Res. 20 (2003) 1337–1350.
[105] H.J. Kuh, S.H. Jang, M.G. Wientjes, J.R. Weaver, J.L. Au, Determinants of paclitaxel penetration and accumulation in human solid tumor, J. Pharmacol. Exp. Ther. 290 (1999) 871–880.
[106] S.M. Mangsbo, L.C. Sandin, K. Anger, A.J. Korman, A. Loskog, T.H. Tötterman, Enhanced tumor eradication by combining CTLA-4 or PD-1 blockade with CpG therapy, J. Immunother. 33 (2010) 225–235.
[107] J. Naidoo, D.B. Page, B.T. Li, L.C. Connell, K. Schindler, M.E. Lacouture, M. A. Postow, J.D. Wolchok, Toxicities of the anti-PD-1 and anti-PD-L1 immune checkpoint antibodies, Ann. Oncol. 26 (2015) 2375–2391.
[108] M.A. Postow, J. Chesney, A.C. Pavlick, C. Robert, K. Grossmann, D. McDermott, G.P. Linette, N. Meyer, J.K. Giguere, S.S. Agarwala, M. Shaheen, M.S. Ernstoff, D. Minor, A.K. Salama, M. Taylor, P.A. Ott, L.M. Rollin, C. Horak, P. Gagnier, J. D. Wolchok, F.S. Hodi, Nivolumab and Ipilimumab versus Ipilimumab in untreated melanoma, N. Engl. J. Med. 372 (2015) 2006–2017.
[109] C.E. Pang, S. Mrejen, Q.V. Hoang, J.A. Sorenson, K.B. Freund, Association between needle size, postinjection reflux, and intraocular pressure spikes after intravitreal injections, Retina 35 (2015) 1401–1406.
[110] E.A. Thackaberry, C. Farman, F. Zhong, F. Lorget, K. Staflin, A. Cercillieux, P. E. Miller, C. Schuetz, D. Chang, A. Famili, A.L. Daugherty, K. Rajagopal, V. Bantseev, Evaluation of the toxicity of Intravitreally injected PLGA microspheres and rods in monkeys and rabbits: effects of depot size on inflammatory response, Invest. Ophthalmol. Vis. Sci. 58 (2017) 4274–4285.
[111] W.M. Saltzman, M.L. Radomsky, Drugs released from polymers: diffusion and elimination in brain tissue, Chem. Eng. Sci. 46 (1991) 2429–2444.
[112] M.F. Haller, W.M. Saltzman, Localized delivery of proteins in the brain: can transport be customized? Pharm. Res. 15 (1998) 377–385.
[113] M. Mak, L. Fung, J.F. Strasser, W.M. Saltzman, Distribution of drugs following controlled delivery to the brain interstitium, J. Neuro-Oncol. 26 (1995) 91–102.
[114] J. Zeng, A.P. See, J. Phallen, C.M. Jackson, Z. Belcaid, J. Ruzevick, N. Durham, C. Meyer, T.J. Harris, E. Albesiano, G. Pradilla, E. Ford, J. Wong, H.J. Hammers, D. Mathios, B. Tyler, H. Brem, P.T. Tran, D. Pardoll, C.G. Drake, M. Lim, Anti-PD-1 blockade and stereotactic radiation produce long-term survival in mice with intracranial gliomas, Int. J. Radiat. Oncol. Biol. Phys. 86 (2013) 343–349.
[115] R. Kuai, L.J. Ochyl, K.S. Bahjat, A. Schwendeman, J.J. Moon, Designer vaccine nanodiscs for personalized cancer immunotherapy, Nat. Mater. 16 (2017) 489–496.